3. Isotopes

3.1 The Periodic System of the Elements

One of the early significant achievements of atomic physics in the past century – or rather, of chemists working together with the physicists – was the explanation of the periodic system of the chemical elements on the basis of atomic structure.

This system (Table 3.1) was first proposed in 1869 by *Medeleev* and independently by *Lothar Meyer*. It is constructed by listing the atoms according to increasing nuclear charge number (or atomic number), Z. In the process, the chemical properties of the atoms are taken into account, so that chemically similar atoms are placed under each other in columns. With this procedure, we find eight vertical columns with subgroups and seven horizontal rows or periods. Each position is occupied by an atom which belongs there because of its chemical properties. To be sure, in this system all fourteen rare earths would have to be placed in the same position, i.e., at $Z = 57$, and all the actinides in position $Z = 89$. Both the periodicity and the above mentioned discrepancies will be explained on the basis of the electronic structure of the atoms near the end of the book in Chap. 19.

Using heavy-ion accelerators, particularly the one operated by the GSI in Darmstadt, Germany, it has been possible to discover additional transuranic elements since 1980. By the end of 1995, elements up to atomic number 111 had been artificially produced. These elements have unstable nuclei and many are so short-lived that their properties are for the most part still unknown; even the process of naming them is as yet unfinished.

The periodic system is an ordering of the elements according to periodically recurring chemical as well as physical properties. As an example of the latter we show here the atomic volumes and the ionisation energies as functions of the nuclear charge Z (Fig. 3.1). Chemical properties which periodically repeat themselves are, for example, the monovalence of the alkali atoms or the lack of reactivity of the rare gases. These empirical regularities indicate corresponding regularities in the atomic structure.

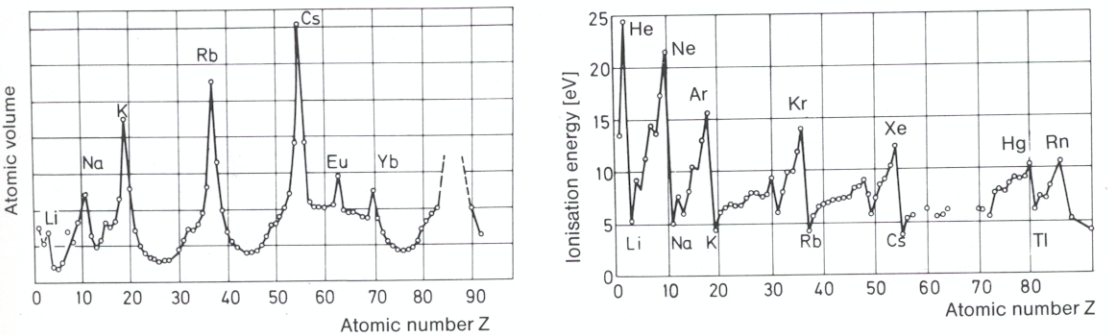

Fig. 3.1. Atomic volumes and ionisation energies as functions of the position in the periodic system of the elements. Particularly noticeable are the (relatively) large atomic volumes of the alkali metal atoms and the large ionisation energies of the noble gas atoms

Table 3.1. Periodic system of the elements

	H 1 1.008															**He** 2 4.0026	
1*s*	1															2	1*s*
	Li 3 6.939	**Be** 4 9.012											**B** 5 10.81	**C** 6 12.01	**N** 7 14.01	**O** 8 16.00	**F** 9 19.00	**Ne** 10 20.18	
2*s*	1	2											2	2	2	2	2	2	2*s*
2*p*	—	—											1	2	3	4	5	6	2*p*
	Na 11 23.00	**Mg** 12 24.31											**Al** 13 26.98	**Si** 14 28.09	**P** 15 30.97	**S** 16 32.06	**Cl** 17 35.45	**Ar** 18 39.95	
3*s*	1	2											2	2	2	2	2	2	3*s*
3*p*	—	—											1	2	3	4	5	6	3*p*
	K 19 39.10	**Ca** 20 40.08	**Sc** 21 44.96	**Ti** 22 47.90	**V** 23 50.94	**Cr** 24 52.00	**Mn** 25 54.94	**Fe** 26 55.85	**Co** 27 58.93	**Ni** 28 58.71	**Cu** 29 63.55	**Zn** 30 65.38	**Ga** 31 69.72	**Ge** 32 72.59	**As** 33 74.92	**Se** 34 78.96	**Br** 35 79.90	**Kr** 36 83.80	
3*d*	—	—	1	2	3	5	5	6	7	8	10	10	10	10	10	10	10	10	3*d*
4*s*	1	2	2	2	2	1	2	2	2	2	1	2	2	2	2	2	2	2	4*s*
4*p*	—	—	—	—	—	—	—	—	—	—	—	—	1	2	3	4	5	6	4*p*
	Rb 37 85.47	**Sr** 38 87.62	**Y** 39 88.91	**Zr** 40 91.22	**Nb** 41 92.91	**Mo** 42 95.94	**Tc** 43 98.91	**Ru** 44 101.07	**Rh** 45 102.9	**Pd** 46 106.4	**Ag** 47 107.9	**Cd** 48 112.4	**In** 49 114.8	**Sn** 50 118.7	**Sb** 51 121.8	**Te** 52 127.6	**I** 53 126.9	**Xe** 54 131.3	
4*d*	—	—	1	2	4	5	6	7	8	10	10	10	10	10	10	10	10	10	4*d*
5*s*	1	2	2	2	1	1	1	1	1	—	1	2	2	2	2	2	2	2	5*s*
5*p*	—	—	—	—	—	—	—	—	—	—	—	—	1	2	3	4	5	6	5*p*
	Cs 55 132.9	**Ba** 56 137.3	**La** 57 138.9	**Hf** 72 178.5	**Ta** 73 181.0	**W** 74 183.9	**Re** 75 186.2	**Os** 76 190.2	**Ir** 77 192.2	**Pt** 78 195.1	**Au** 79 197.0	**Hg** 80 200.6	**Tl** 81 204.4	**Pb** 82 207.2	**Bi** 83 209.0	**Po** 84 (210)	**At** 85 (210)	**Rn** 86 (222)	
5*d*	—	—	1	2	3	4	5	6	7	9	10	10	10	10	10	10	10	10	5*d*
6*s*	1	2	2	2	2	2	2	2	2	1	1	2	2	2	2	2	2	2	6*s*
6*p*	—	—	—	—	—	—	—	—	—	—	—	—	1	2	3	4	5	6	6*p*
	Fr 87 (223)	**Ra** 88 (226)	**Ac** 89 (227)	**Ku** 104 (258)	**Ha** 105 (260)														
6*d*	—	—	1	2?	3?														
7*s*	1	2	2	2?	2?														
7*p*	—	—	—	—	—														

	Ce 58 140.1	**Pr** 59 140.9	**Nd** 60 144.2	**Pm** 61 (145)	**Sm** 62 150.4	**Eu** 63 152.0	**Gd** 64 157.3	**Tb** 65 158.9	**Dy** 66 162.5	**Ho** 67 164.9	**Er** 68 167.3	**Tm** 69 168.9	**Yb** 70 173.0	**Lu** 71 175.0	
4*f*	2	3	4	5	6	7	7	8	10	11	12	13	14	14	4*f*
5*d*	—	—	—	—	—	—	1	1	—	—	—	—	—	1	5*d*
6*s*	2	2	2	2	2	2	2	2	2	2	2	2	2	2	6*s*
	Th 90 232.0	**Pa** 91 231.0	**U** 92 238.0	**Np** 93 237.0	**Pu** 94 239.1	**Am** 95 (243)	**Cm** 96 (247)	**Bk** 97 (247)	**Cf** 98 (251)	**Es** 99 (252)	**Fm** 100 (257)	**Md** 101 (258)	**No** 102 (259)	**Lr** 103 (260)	
5*f*	—	2	3	5	6	7	7	9	10	11	12	13	14	14	5*f*
6*d*	2	1	1	—	—	—	1	—	—	—	—	—	—	1	6*d*
7*s*	2	2	2	2	2	2	2	2	2	2	2	2	2	2	7*s*

—Element and atomic number
—Atomic mass in u; for some unstable elements, the mass number of the most stable isotope is given in parentheses.
Electron configuration; the filled shells of the previous periods are not shown. For example, the complete electron configuration of Fe is $1s^2 2s^2 2p^6 3s^2 3p^6 3d^6 4s^2$

A first attempt at an explanation was the hypothesis of *Prout* (1815): all atoms are made up of hydrogen atoms. This picture was refined and modified as further elementary particles were discovered, first the electron, then the proton. Only after 1932 did it become clear that the atomic nucleus consists of neutrons as well as protons. The number of electrons of an atom is smaller than the mass number, since the nucleus contains just as many protons as the electronic shells have electrons, but it also contains neutrons.

The relative atomic masses A_{rel} could originally only be measured by chemical methods. By these means, it was determined that the addition of hydrogen atoms alone cannot explain the observed "atomic weights" without contradictions. If the model of Prout is correct, then the atomic weights must be integers. For the most part, they *are* integers to a good approximation; A and A_{rel} are nearly equal. However, there are counter examples: the relative atomic mass – the atomic weight – of chlorine, for example, is $A_{rel} = 35.5$ in the naturally occurring element. Furthermore, it was determined that lead from various ores had differing atomic weights. Today we know that this is due to the lead having been produced as the end product from different radioactive decay chains.

These observations were the starting point for investigations which led to the discovery of the *isotopes*. This term denotes the fact that atoms with differing mass numbers may belong to the same position in the periodic table, i.e., they may have the same nuclear charge number Z. The position of an element in the Periodic Table is determined by the number of protons in its atomic nucleus. The differing mass numbers result from the different numbers of neutrons in the atomic nuclei. The concept of isotopes will be treated in the following sections. The existence of isotopes was discovered and thoroughly investigated with the aid of *mass spectroscopy*.

3.2 Mass Spectroscopy

3.2.1 Parabola Method

The physical techniques for exact measurement of atomic masses and for separating atoms with differing masses are mostly methods for determining the ratio e/m, i.e., the ratio of charge to mass. For this purpose one uses the deflection of ionized atoms moving through electric fields $\boldsymbol{E}$ and magnetic fields $\boldsymbol{B}$.

The oldest and most easily understood method is the parabola method of *Thomson* (1913). An ion beam from a gas discharge passes through the electric field of a condenser and a magnetic field $\boldsymbol{B}$ which is oriented parallel to the electric field (Fig. 3.2). In the plane of observation, particles of the same charge and mass, but having different velocities v, are distributed along a parabola whose origin is in the point where the undeflected beam would pass. This can be shown in the following manner: The homogeneous electric field $\boldsymbol{E}$, which is applied in the y direction, causes a deflection in this direction. The y coordinate of the particles changes according to the equation for the acceleration:

$$\ddot{y} = (e/m) \cdot E \,. \tag{3.1}$$

The y coordinate itself is given by the solution of (3.1),

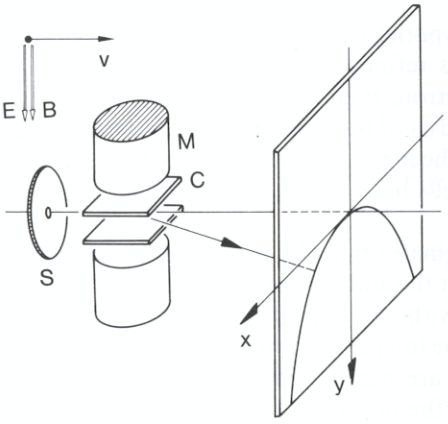

Fig. 3.2. Schematic representation of the parabola method. The ion beam, collimated by the slit S, is deflected by the magnet M and the condenser C in the x and y directions. Equation (3.5) describes the path of the particles on a catcher screen immediately after exiting from the magnet and the condenser. If the screen is placed at a greater distance, a corresponding distortion of the parabolas due to projection is seen. Both branches of the parabola are valid solutions if the **B** field is allowed to change its sign

$$y = \frac{1}{2}\,\frac{eE}{m}\,t^2 = \frac{e}{2m}\,E \cdot \frac{l^2}{v^2}\,, \tag{3.2}$$

where the last equation is found by expressing the time spent by the particles in the electric field in terms of the velocity v and the length l of the condenser. This is permitted as long as the magnetic field $\boldsymbol{B}$ is sufficiently weak and thus the radius $\boldsymbol{r}$ is sufficiently large. Since the deflection of the particles in the y direction is inversely proportional to the kinetic energy $mv^2/2$, the condenser is referred to as an *energy filter*.

The homogeneous $\boldsymbol{B}$ field, which is also applied in the y direction, produces a deflection in the x direction. This deflection can be calculated as follows:

The particles which enter the homogeneous $\boldsymbol{B}$ field are forced to follow circular orbits in a plane perpendicular to the direction of the field (y direction). Since, however, the $\boldsymbol{B}$ field is limited in spatial extent (Fig. 3.2), the particles pass through only a segment of this circular orbit and then move on in a straight line. The resulting deflection in the x direction may be derived by means of the radius of curvature of the circular orbit, which is obtained by setting equal the magnitudes of the Lorentz force in the magnetic field, $\boldsymbol{F} = e(\boldsymbol{v} \times \boldsymbol{B})$, and of the centrifugal force $\boldsymbol{F}_c = mv^2\boldsymbol{r}/r^2$:

$$r = mv/eB\,. \tag{3.3}$$

For the centrifugal acceleration $a_c = v^2/r$ we obtain [by inserting (3.3) for the radius] the following relation:

$$a_c = eBv/m\,.$$

Since the particle only moves through a relatively short segment of the circle, we may replace its acceleration in the x direction with the centrifugal acceleration a_c. The total deflection in the time t is given by

$$x = a_c t^2/2\,.$$

In this equation, we replace a_c by eBv/m and the time of flight t by the quotient l/v, where l is the distance traveled in the field. We then obtain for the deflection in the x direction

$$x = \frac{eBl^2}{2mv}\,. \tag{3.4}$$

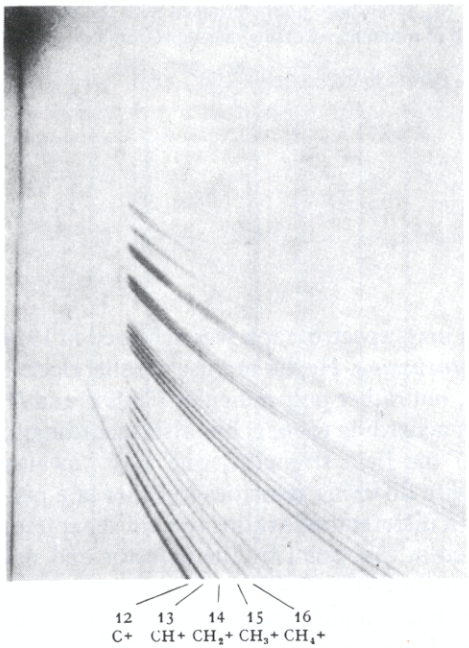

Fig. 3.3. Separation of a mixture of hydrocarbon ions with the Thomson parabola method. For calibration, one uses ions of known mass. The intensities of the individual parabolic sections correspond to the relative amounts within the mixture of the ions which produced them. [Photo after *Conrad* from W. Finkelnburg: *Einführung in die Atomphysik*, 11, 12th ed. (Springer, Berlin, Heidelberg, New York 1976) Fig. 12]

The x deflection is inversely proportional to the momentum mv of the particles. For this reason, one often calls the magnet causing the deflection a *momentum filter*. From the expressions for x and y we can eliminate v, so that we obtain the equation for the orbit of deflection of the particles:

$$y = \frac{2E}{l^2 B^2} \cdot \frac{m}{e} x^2. \tag{3.5}$$

This is the equation of a parabola $x^2 = 2py$ with the parameter $p = el^2B^2/4mE$. This parameter has the same value for ions with the same ratio m/e but with differing velocities v. An example of a measurement is shown in Fig. 3.3.

The total intensity of the partial beam which produces a particular parabola is a measure of the relative abundance of the corresponding ion or isotope. Since the ions in general have differing velocities due to their preparation in an oven or a gas discharge tube, those ions having the same values of m/e will be distributed over the entire length of a particular segment of a parabola.

Aston used this method in 1920 to investigate the composition of naturally occurring neon, which consists of 3 types of atoms with the mass numbers 20, 21, and 22; this was the first exact demonstration of the existence of isotopes by means of mass spectroscopy (Table 3.2).

In any case, the most important result of the measurements with the parabola method was the following: many elements consist of several *isotopes*, that is atoms with the same nuclear charge number Z and differing mass numbers A. Nuclei with particular values of A and Z are referred to as *nuclides*.

Table 3.2. Isotopic composition of neon. The values of A_{rel} given were not determined with the parabola method, but rather, with the precision quoted, by the use of a double-focussing mass spectrometer

$^{20}_{10}$Ne	90.92%	$A_{rel} = 19.99244$
$^{21}_{10}$Ne	0.26%	$A_{rel} = 20.99385$
$^{22}_{10}$Ne	8.82%	$A_{rel} = 21.99138$

3.2.2 Improved Mass Spectrometers

The first essential improvement of *Thomson*'s mass spectrograph was achieved in 1919 by *Aston*, namely the introduction of *velocity focussing*. He did not use parallel electric and magnetic fields as in the parabola method, but rather perpendicular fields $\boldsymbol{E}$ and $\boldsymbol{B}$. The $\boldsymbol{E}$ field splits up the incident particle beam according to m/e, but also according to different velocities. By proper adjustment of the field strengths, one may however ensure that the $\boldsymbol{B}$ field brings all the particles with differing velocities together at a particular point in space, while particle beams with different m/e ratios remain separated. Particles with the same m/e ratio are collected at one point by the detector and not along a parabolic segment as in the parabola method (Fig. 3.4).

An apparatus with velocity focussing thus has a higher transmission for the ions than one which uses the simple parabola method, i.e., one can detect smaller amounts of ions and so, by closing down the slits, obtain a better mass resolution. The resolution attained by *Aston* (1919) was about 130 for the ratio $m/\Delta m$, that is, for the mass divided by the separable mass difference Δm.

The second major improvement was the introduction of directional focussing (first done by *Dempster* in 1918). By means of properly dimensioned sector fields (Fig. 3.5), it can be ensured that ions with the same m/e ratio but with somewhat differing angles of incidence, which are therefore deflected by differing amounts, are again collected at a point.

In modern high-resolution mass spectrographs, both methods – velocity and directional focussing – are used, leading to what is called *double focussing*. The precision attainable today for the relative atomic masses A_{rel} is down to 10^{-7} u. The same criteria apply as for optical spectrographs: by using narrow slits one obtains high resolution,

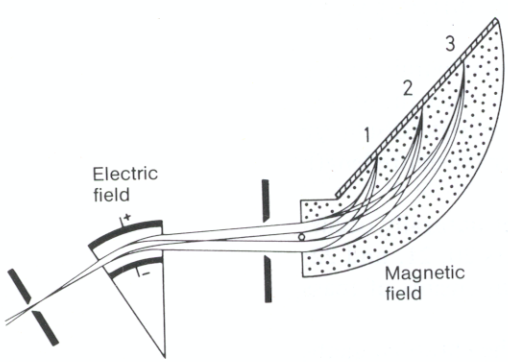

Fig. 3.4. A focussing mass spectrograph as designed by *Aston*. The points 1, 2, and 3 denote the points at which three types of particles with three different values of m/e are collected

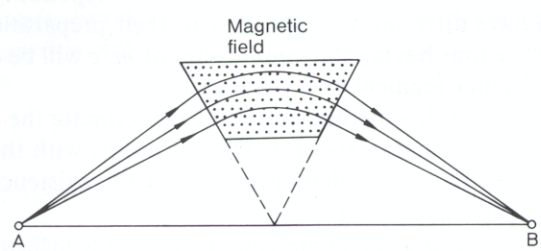

Fig. 3.5. Directional focussing in a magnetic sector field, schematically illustrated. Particles which pass a longer distance through the region of magnetic field are more strongly deflected

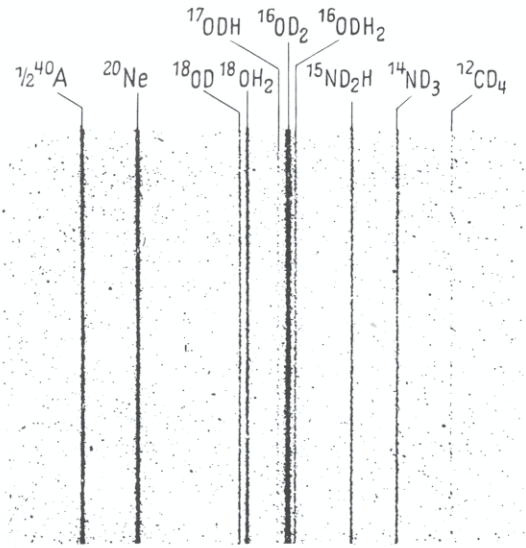

Fig. 3.6. An example of high-resolution mass spectroscopy: separation of 10 different ions with mass number 20, whose atomic or molecular weights lie between 19.9878 and 20.0628. The picture was made with the double-focussing mass spectrometer of *Mattauch* and coworkers [from W. Finkelnburg: Einführung in die Atomphysik, 11, 12th ed. (Springer, Berlin, Heidelberg, New York 1976) Fig. 15]

but at the cost of intensity. This represents the principal problem for the experimentalist. The high resolution is mainly needed for nuclear physics problems, e.g., for the measurement of the so-called mass defect, but also for problems in analysis and structure determination in chemistry, Sect. 3.2.4. The resolution $m/\Delta m$ which can be attained at present, i.e., the possibility of separating two masses with the values m and $m+\Delta m$, is more than 100000. An example is shown in Fig. 3.6.

3.2.3 Results of Mass Spectrometry

In atomic physics, mass spectrometers are primarily of interest as instruments for analysing the isotopic composition of chemical elements.

An element often has several isotopes, for example chlorine: an isotope with mass number 35 occurs with an abundance of 75.4%; the other stable isotope with mass number $A = 37$ has an abundance of 24.6%. The resulting relative atomic mass of the isotope mixture is $A_{\text{rel}} = 35.457$. There are elements with only one stable isotope, for example

$$^{9}_{4}\text{Be},\ ^{27}_{13}\text{Al},\ ^{127}_{53}\text{I},$$

and others with two stable isotopes, e.g.,

$$^{1}_{1}\text{H} \qquad ^{2}_{1}\text{H}$$
$$99.986\% \qquad 0.014\%,$$

and finally there are elements with many stable isotopes. For example, mercury, $_{80}$Hg, has 7 stable isotopes with A between 196 and 204. A few further examples are contained in Table 3.3.

Table 3.3. Some examples of isotopes

	Mass number	Rel. atomic weight	Abs. atomic weight [10^{-27} kg]
^{1}H	1	1.007825	1.67342
^{2}H	2	2.014102	3.34427
^{12}C	12	12.000000	19.9251
^{16}O	16	15.99415	26.5584
^{35}Cl	35	34.96851	58.0628
^{37}Cl	37	36.965898	61.37929

3.2.4 Modern Applications of the Mass Spectrometer

Aside from precision measurements in atomic and nuclear physics, mass spectrometers with limited mass resolution are utilised today in many applications in science and technology.

In chemistry, simplified double-focussing spectrometers are used for analytical purposes. The molecular fragments which result from electron or ion bombardment of molecules are identified; from their distribution, a clue to the identification of the original molecules is obtained.

In physics, chemistry, and technology, simple, compact spectrometers are used to analyse residual gases in vacuum systems. For this purpose, a mass resolution of $m/\Delta m = 100$ is usually sufficient.

A further application of these relatively simple spectrometers is the production of pure atomic and molecular beams. Recently, high-frequency mass spectrometers have been applied for this purpose. In these so-called time-of-flight spectrometers, charged particles are differently accelerated by high-frequency electromagnetic fields depending on their specific charges, and pass through the spectrometer with different velocities. The different times of flight (through the spectrometer) are a measure of the ratio e/m.

In a quadrupole mass filter, the superposition of direct and alternating potentials on the four cross-connected, parabolically shaped electrodes results in an inhomogeneous high-frequency field in the interior of the electrode assembly. A static field is superposed on the high-frequency field. Only particles with a particular mass and energy can pass through a filter with a given geometry and frequency (Fig. 3.7).

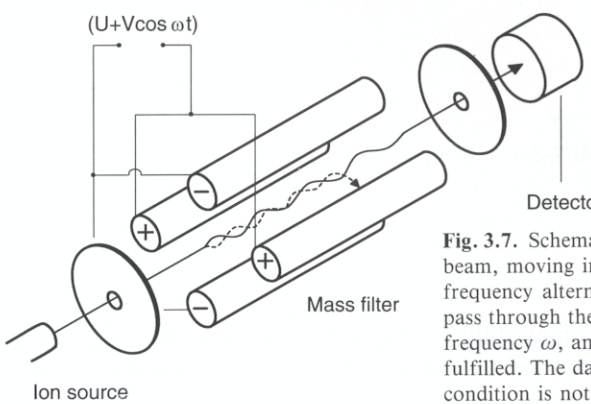

Fig. 3.7. Schematic of a quadrupole mass filter. The ion beam, moving in the $+z$ direction, is deflected by a high-frequency alternating potential. In order for the beam to pass through the filter, a certain relation between e/m, the frequency ω, and the deflection voltages U and V must be fulfilled. The dashed orbit applies to an ion for which this condition is not met

3.2.5 Isotope Separation

The separation of isotopes is more a problem of technology and nuclear physics than of atomic physics, which is the main topic of this book. For this reason, we will only briefly treat the subject here.

In principle, any method which can distinguish particles on the basis of a physical property depending on the mass may be used to separate isotopes. Which one is employed in a particular application depends on questions of economics and the state of the technology. The requirements are rather varied.

Separation of the two hydrogen isotopes ${}^{1}_{1}\mathrm{H}$ and ${}^{2}_{1}\mathrm{H}$ with a mass difference of 100% is relatively easy, while by contrast the separation of ${}^{235}_{92}\mathrm{U}$ and ${}^{238}_{92}\mathrm{U}$ is considerably more difficult. In the latter case, the masses differ by only 1.25%. In the following, the most important methods will be briefly described.

Electromagnetic separation with mass spectrographs is usually expensive and slow. The yields which can be obtained are of the order of 1 mg per hour at a current of 10^{-4} A. For example, 35 g Cl as singly charged ions corresponds to 96500 As transported charge. At a current of 10^{-4} A, 35 g of Cl will be deposited in a time

$$\frac{9.65 \cdot 10^{4}\,\mathrm{As}}{10^{-4}\,\mathrm{A}} = 9.65 \cdot 10^{8}\,\mathrm{s} = 30\ \text{years}\,.$$

Nevertheless, this technique is applied on a large scale for isotope separation, for example for separating uranium isotopes, initially for the manufacture of uranium fission bombs. The necessary investment of technology and energy is enormous.

Mass separation by means of *diffusion* through porous membranes is based on the fact that in a gas, particles of differing masses m_1 and m_2 have different velocities v_1 and v_2 at a given temperature. The following relation holds:

$$v_1/v_2 = \sqrt{m_2/m_1}\,, \quad \text{since} \quad m_1 v_1^2 = m_2 v_2^2\,,$$

that is, the mean kinetic energy for both types of particle is the same. Light atoms are therefore on the average faster and diffuse more quickly. To obtain efficient isotope separation, many diffusion layers must be connected in series. This method was at first the most important technology for uranium separation: the gaseous compound UF_6 is employed to enrich the uranium isotope ${}^{235}_{92}\mathrm{U}$ relative to ${}^{238}_{92}\mathrm{U}$.

The *gas centrifuge* is also applied on a large scale for uranium separation. Here, the heavier isotope is acted upon by a stronger centrifugal force. The lighter isotope is enriched in the region of the centrifuge axle. For effective separation, many stages must be employed one after another. The most serious technical problem is the strength of the materials used in view of the extreme accelerations necessary.

The *separation tube* utilises thermodiffusion: it is based on the principle that a temperature gradient in a mixture of gases leads to a separation of the mixture; the effect is increased by convection. Along the axis of a long tube, a heater wire is suspended. The lighter isotope is enriched by thermal diffusion in the middle and at the top, the heavier isotope collects by convection at the outer wall and at the bottom of the tube.

Fractional distillation in repeated steps uses the fact that the heavier isotope in general has the higher boiling point. For example, the boiling point of heavy water (D_2O) lies 1.42 degrees above that of H_2O.

In *electrolysis*, molecules with the heavier isotope are less easily decomposed than those with the lighter isotope. This technique is used for large-scale separation of heavy and light hydrogen.

There are also *chemical reactions* in which molecules with differing isotopic compositions react with different rates. In such cases, isotope separation can be achieved through chemical reaction. Since the availability of narrow-band, tunable light sources in the form of dye lasers, (see Chap. 21), *laser photochemistry* can also be used for isotope separation. In this method, certain isotopes in a mixture of molecules composed of various isotopes can be selectively photoexcited, leading to photochemical reactions of the selected molecules. Some interesting new techniques for isotope separation have been developed in recent years based on this principle.

Problems

3.1 Show that a transverse homogeneous magnetic field can be used to sort charged particles according to their momenta, and to sort monoenergetic particles according to their masses. All the particles have the same charge.

3.2 An ion beam containing $^1H^+$, $^2H^+$, and $^3H^+$ is accelerated through a voltage of 1000 V and is directed perpendicular to the field lines of a 0.05 tesla magnetic field. How far apart are the component beams when they have travelled 5 cm through the homogeneous magnetic field and are measured at a distance of 25 cm from the beginning of the magnetic field?

3.3 A beam of positive ions traverses for a distance $l = 4$ cm an electric field $|\boldsymbol{E}| = 5000$ V/m and a parallel magnetic field $|\boldsymbol{B}| = 0.01$ tesla. The ions travel perpendicular to the direction of the two fields (parabola method). They then cross a field-free region $l' = 18$ cm and land on a flat fluorescent screen. What are the parameters of the parabolas on the screen if the beam consists essentially of singly charged hydrogen ions and hydrogen molecules with a velocity corresponding to an accelerating voltage between 1000 V and 4000 V? What does the image on the screen look like if both positively and negatively charged ions are directed at it?

3.4 The isotopic abundance of ^{235}U and ^{238}U in naturally occurring uranium is 0.72% and 99.28%, respectively. If the isotopes are separated by diffusion, the isotopic mixture after one separation step is 0.754% ^{235}U. How many separations are needed to enrich the ^{235}U to 50%? to 99%?

Hint: The separation coefficient α = (relative concentration before separation)/(relative concentration after separation) is independent of the composition of the isotopic mixture.

4. The Nucleus of the Atom

4.1 Passage of Electrons Through Matter

Beginning in the 1890s, *Lenard* investigated the attenuation of electron beams passing through matter. This attenuation can have two causes: the electrons can lose their energy by exciting or ionising atoms, or they can be elastically scattered and so change their directions and leave the beam. *Lenard* produced the beam by means of a cathode ray tube. Today, one would use thermionic emission as the electron source.

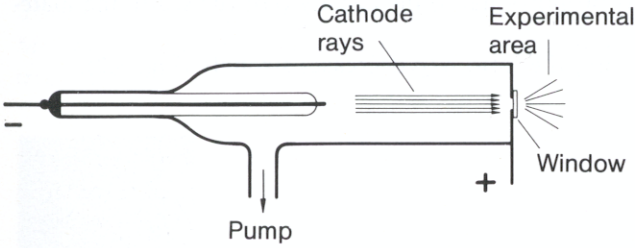

Fig. 4.1. Schematic of *Lenard*'s cathode ray tube. The cathode rays pass through a thin foil – the Lenard window – into the surrounding air and excite it, producing fluorescence

An important result may be obtained from the qualitative experiment illustrated in Fig. 4.1: if the gas discharge tube used for producing the cathode rays is closed with an extremely thin aluminium foil, it may be observed that electrons from the cathode ray beam pass through the foil. They excite the air for a distance of several centimeters outside the tube, yielding a bluish-red fluorescence light, and can be detected several cm away from the end of the tube by using a fluorescent screen. An aluminium window of this type, with a thickness of ca. $5 \cdot 10^{-4}$ cm, is called a *Lenard window*. The experiment offers visible proof that the electrons can pass through some 10000 atomic layers as well as several cm of air at NTP. Under the assumption that atoms were impenetrable for electrons, the scattering of electrons by air would take place over a length of the order of the gas kinetic mean free path, i.e., in a range of about 10^{-5} cm.

From such qualitative experiments, it follows that the interaction cross section for collisions of an electron from a gas discharge tube with atoms is small compared to the cross section for collisions between two atoms.

For the quantitative determination of the interaction cross section between electrons and atoms, one may employ a setup analogous to that shown in Fig. 4.1, where, however, the cathode ray beam passes through the Lenard window into a scattering chamber. In the chamber, the electron current is measured after the beam has passed through a gas atmosphere of known composition and density. The collisions of the electrons with the atoms in the foil can also be investigated; for this purpose, the experimental parameters (foil thickness, foil material, pressure and composition of the gas, and distance between foil and electron detector) may all be varied. The interaction

cross section is obtained from the ratio of incident (I_0) and transmitted (I) electron intensities by means of the equation derived above (2.22):

$$I(x) = I_0 e^{-\alpha x}, \tag{4.1}$$

where x indicates the thickness of the scattering layer.

It may be shown that:

- The *absorption* or *scattering coefficient* α is proportional to the pressure in the scattering chamber. This is in agreement with the definition of the total interaction cross section given earlier as being equal to the sum of the partial cross sections, $\alpha = \sum_{i=1}^{n} \sigma_i$, since, for identical scattering particles, $\alpha = \sigma n$ is then the sum of all the interaction cross sections per unit volume, where n gives the number of particles per unit volume and is proportional to the gas pressure.
- In foils and in gases, *independent of the phase of matter and of the particular properties of the material*, for a given electron velocity it is found that $\alpha/\varrho = \text{const}$, i.e., the interaction cross section is proportional to the density ϱ of the scattering material.
- With increasing electron velocity, the ratio α/ϱ decreases strongly (Fig. 4.2).

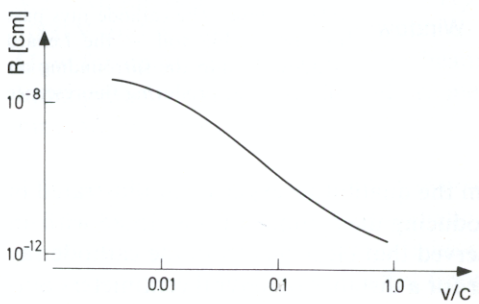

Fig. 4.2. Qualitative behaviour of the interaction cross section for gas atoms and electrons as a function of the electron velocity. The collision radius R, which is connected with the cross section σ by means of $\pi R^2 = \sigma$ (Sect. 2.4.2), is plotted against the ratio v/c of the electron velocity to the velocity of light

In Fig. 4.2, the collision radii calculated from the measured interaction cross sections α are plotted as a function of the electron velocity. For very fast electrons, atoms are thus a factor of 10^8 more penetrable than for slow electrons. The experiments lead to the following conclusion: only a small portion of the atomic volume is impenetrable for fast electrons, or, as expressed by *Lenard* – the inside of an atom is as empty as interplanetary space.

At first, the only general conclusion which could be drawn from this result was that the mass and charge in an atom are distributed in a "lumpy" fashion, rather than being evenly spread throughout the atomic volume. *Lenard* spoke of nuclei and force fields. The analogy with a solar system was tempting. Today, we know that slow electrons are scattered by the atomic electron cloud, while fast electrons are scattered by the nucleus only.

The realisation that there is *one* small nucleus, which contains the entire positive charge and almost the entire mass of the atom, is due to the investigations of *Rutherford*, who utilised the scattering of alpha particles by matter.

4.2 Passage of Alpha Particles Through Matter (Rutherford Scattering)

4.2.1 Some Properties of Alpha Particles

Alpha particles are emitted by some radioactive nuclei. They consist of doubly ionised helium nuclei, $^4_2He^{2+}$, with high kinetic energies (several MeV). They can, for example, be detected by means of their ability to ionise air in a cloud chamber; alpha particles with an energy of 5 MeV have a range of about 3.5 cm in air at NTP. In this distance, they lose their initial kinetic energy to the air molecules through ionisation and excitation processes. Since the mean free path for atoms or molecules as calculated by the kinetic theory of gases amounts to about 10^{-5} cm, we see that alpha particles can penetrate and pass through thousands of atoms ($3.5\text{ cm}/10^{-5} \triangleq 3.5 \cdot 10^5$ atoms) without being noticeably deflected from a straight path. Cloud chamber pictures show that the paths of the alpha particles are for the most part straight; only near the ends of the tracks, when the particles have lost most of their kinetic energy and are moving slowly, do we observe large deflections from straight-line paths (Fig. 4.3). Another possibility for observing the paths of alpha particles is offered by the spinthariscope or the scintillation detector (Figs. 2.16 and 2.17). Using scintillation detectors, *Geiger* and *Marsden* investigated the scattering of alpha particles in matter, which we will now treat in detail.

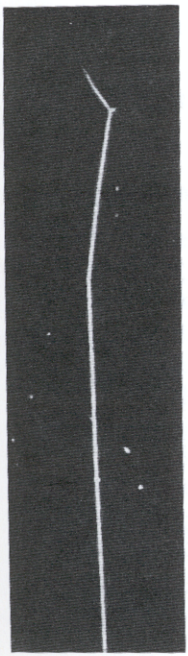

Fig. 4.3. Cloud chamber photograph of the track of an alpha particle, by *Wilson*. The particle passes through several cm of air without noticeable deflection. At the end of the track, we see two deflections; at the second, we can also see the short track of the target nucleus, which was accelerated to the right by the collision. [From W. Finkelnburg: *Einführung in die Atomphysik*, 11,12th ed. (Springer, Berlin, Heidelberg, New York 1976) Fig. 3]

4.2.2 Scattering of Alpha Particles by a Foil

In order to investigate the interaction cross section for collisions between alpha particles and atoms quantitatively, *Rutherford* and coworkers utilised the following experimental setup (Fig. 4.4):

The alpha particles, which are emitted by naturally radioactive material R, pass through a collimator and strike a thin metal foil F. The transmitted alpha intensity is determined by means of a scintillation screen S, observed through the lens L. In contrast to the determinations of interaction cross sections described above, in *Rutherford*'s experiments the directly transmitted alpha intensity was not the main object of the investigation; instead, the dependence of the scattered intensity on scattering angle θ was determined. θ is the angle between the directions of the deflected and the incident particle beams (Fig. 4.7). Scattering experiments of this type have become one of the most important tools in nuclear physics. A typical experiment yields a result like the one shown in Fig. 4.5.

The scattered intensity decreases strongly with increasing scattering angle. The angular dependence is well described by the inverse fourth power of the sine of half the scattering angle. At large scattering angles, deviations from this dependence are seen; we will treat this so-called anomalous Rutherford scattering in Sect. 4.2.4.

It is further observed that scattering occurs even at very large angles. It can be concluded that this is not due to multiple scattering processes; in scattering of alpha particles by helium atoms in a cloud chamber, large deflection angles, namely 90°, can be seen directly. An example is shown in the cloud chamber photograph in Fig. 4.6.

A quantitative explanation of these results may be given with the help of the Rutherford atomic model (1911). The model states that:

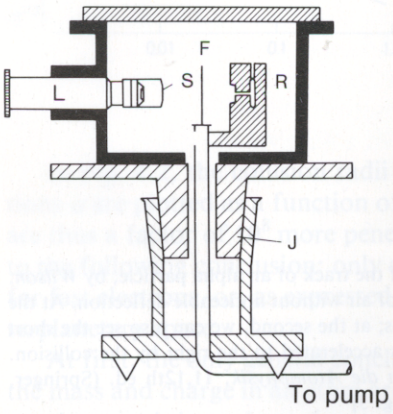

Fig. 4.4. Experimental setup for the investigation of Rutherford scattering: alpha particles from the radioactive source R are scattered by the foil F. The light flashes which are produced by the scintillation screen S are observed through the observation telescope L. The chamber can be evacuated and the observation lens L may be turned around the foil axis by means of the ground-glass joint J

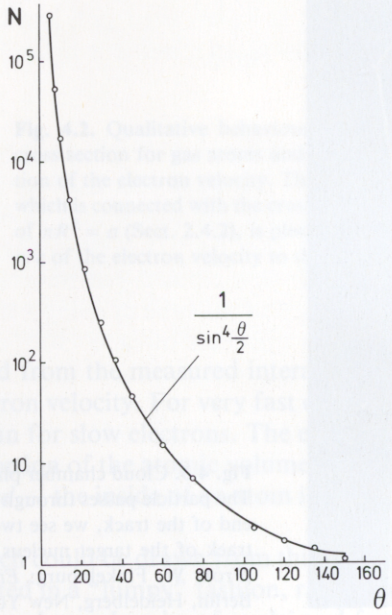

Fig. 4.5. Graphical representation of the experimental results of *Geiger* and *Marsden* for the Rutherford scattering of alpha particles by a gold foil. The scattering rate N is plotted as a function of the scattering angle θ. The solid curve represents the theoretical function for Coulomb scattering

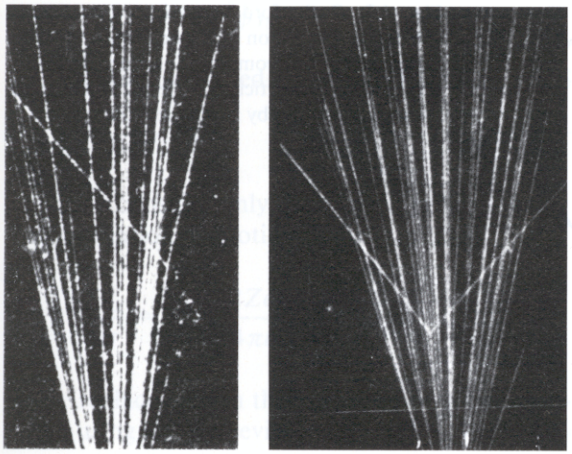

Fig. 4.6. Cloud chamber photographs of alpha particles. Collision processes with the gas in the chamber can be seen; *left*, the chamber gas is hydrogen, *right*, it is helium. In hydrogen, the alpha particle is only slightly deflected from a straight-line track, while the hydrogen target nucleus recoils sharply off to the left. In helium, the angle between the tracks of the alpha particle and the recoiling nucleus after the collision is 90°, since the two particles have the same mass. [From K. H. Hellwege: *Einführung in die Physik der Atome*, Heidelberger Taschenbücher, Vol. 2, 4th ed. (Springer, Berlin, Heidelberg, New York 1974) Fig. 4]

- Atoms have nuclei with a radius R of about 10^{-12} cm. The nucleus contains nearly the entire mass of the atom. A collision between an alpha particle and a much lighter atomic electron produces no measurable deflection in the alpha particle's path.
- The atomic nucleus has a positive charge Ze, where Z is the position of the element in the periodic table.
- Around the positively charged nucleus is a Coulomb field given by (at distance r)

$$E = (1/4\pi\varepsilon_0)\frac{Ze}{r^2}\frac{r}{r}. \tag{4.2}$$

4.2.3 Derivation of the Rutherford Scattering Formula

The above model leads to the Rutherford scattering formula (4.20) if we take into account only the Coulomb repulsion between the nuclear charge and the charge of the alpha particle. We will use the model to calculate the dependence of the scattering probability on the deflection angle in two steps: first, for a single scattering event we determine the dependence of the deflection angle on the *impact parameter b*, which is the distance of closest approach of the alpha particle to the target nucleus, assuming no deflection occurs (see Fig. 4.7). We shall see that a unique relation between the impact parameter b and the deflection angle θ exists. Secondly, we will average over all possible impact parameters, since we cannot follow a single alpha particle on its path through the target foil, but rather observe the scattering of many alpha particles. Multiple scattering will not be considered; for the experiment, this means that the target foil must be sufficiently thin that each alpha particle is only scattered once on passing through the target.

In order to calculate the path of the particle we recall the motion of a planet under the influence of an attractive gravitational field. The effective force is proportional to $1/r^2$ where r is the sun-planet distance. The orbits which one finds in this case are known to be either elliptical, parabolic, of hyperbolic.

Since the Coulomb force has the same dependence upon distance r as the gravitational force, the orbital calculations from celestial mechanics can be utilised directly. Admittedly, since the Coulomb force is here repulsive, only the hyperbolic orbits represent possible solutions when we are dealing with charges of the same signs.

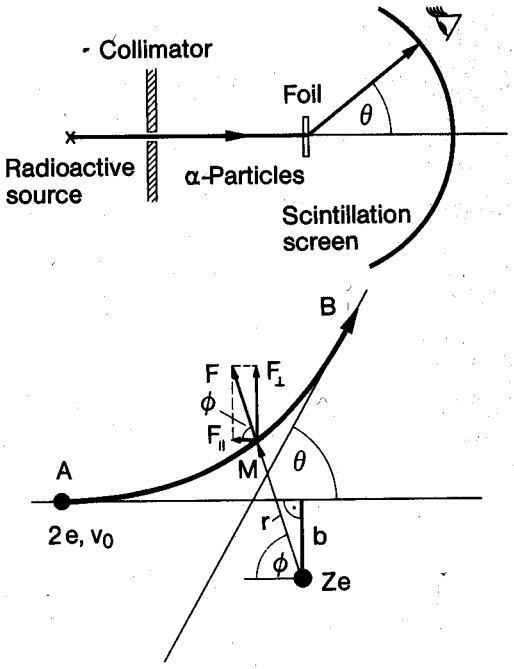

Fig. 4.7. Rutherford scattering. *Upper part:* Schematic illustration of the experimental setup. *Lower part:* The geometry of the model calculation. The alpha particle is deflected from A to B through scattering by the nucleus Ze

We now wish to determine the relation between the scattering angle θ and the impact parameter b (Fig. 4.7). The particle arrives at point A, still distant from the nucleus, with a velocity v_0. If it were not deflected, it would pass the nucleus at a distance b. Between the alpha particle and the nucleus, there is a repulsive Coulomb force F

$$F = \frac{2Ze^2}{4\pi\varepsilon_0 r^2}\,\frac{r}{r} \tag{4.2a}$$

with the nuclear charge Ze, the elementary charge e, the permittivity constant ε_0, and a distance r between the nucleus and the alpha particle.

We assume that the particle has reached point M in its orbit and express the force which acts there in terms of two components:

$$F_\perp = F\sin\phi \quad \text{perpendicular to the original direction}, \tag{4.3}$$

and

$$F_{\parallel} = F\cos\phi \quad \text{antiparallel to the original direction}. \tag{4.4}$$

ϕ is the angle between the horizontal (i.e., the direction of the incident beam) and the radius vector r to the momentary position of the particle.

We now apply the law of conservation of angular momentum, placing the origin of the coordinate axes at the centre of the atomic nucleus. Since the force which acts here is radial (4.2a), it produces no torque and the angular momentum is constant; in particular, the angular momenta at the points A and M are the same, or, mathematically,

$$(mv_0 b)_A = (mr^2\dot{\phi})_M \tag{4.5}$$

in which we have used polar coordinates (r, ϕ). Solving for $1/r^2$ yields

$$1/r^2 = \dot{\phi}/v_0 b\,. \tag{4.6}$$

If we consider only the motion perpendicular to the original beam direction, Newton's equation of motion reads

$$m\frac{dv_\perp}{dt} = F_\perp = \frac{2Ze^2}{4\pi\varepsilon_0}\frac{1}{r^2}\sin\phi\,. \tag{4.7}$$

If we replace $1/r^2$ in this equation with the right-hand side of (4.6) and integrate over time, using the abbreviation $k = 2Ze^2/4\pi\varepsilon_0$, we obtain

$$\int_{t_A}^{t_B}\frac{dv_\perp}{dt}\,dt = \frac{k}{mv_0 b}\int_A^B \sin\phi\frac{d\phi}{dt}\,dt\,. \tag{4.8}$$

In order to determine the limits of the integral, we imagine the point A to be infinitely distant from the nucleus. Since now no Coulomb force acts, we have $v_\perp = 0$, and the angle $\phi = 0$.

To determine the scattering angle θ between the incident direction and the direction of the particle after scattering, we let point B (see Fig. 4.7) move away to infinity. Then the angle ϕ is seen to be related to θ through the expression $\phi = 180° - \theta$. Because of conservation of energy, the final velocity at the point B is equal to the initial velocity v_0 at point A, since the potential energy vanishes at a sufficiently large distance from the nucleus. The component $v_\perp$ has, using $\phi = 180° - \theta$, the value $v_\perp = v_0 \sin\theta$. Then the integral equation (4.8) becomes, using

$$\frac{dv_\perp}{dt}\,dt = dv_\perp \quad \text{and} \quad \frac{d\phi}{dt}\,dt = d\phi\,,$$

the following equation:

$$\int_0^{v_0\sin\theta} dv_\perp = \frac{k}{mv_0 b}\int_0^{\pi-\theta}\sin\phi\,d\phi\,. \tag{4.9}$$

Upon integration, we obtain

$$v_0\sin\theta = \frac{k}{mv_0 b}(1+\cos\theta)\,. \tag{4.10}$$

With the trigonometric identity

$$\frac{1+\cos\theta}{\sin\theta} = \cot(\theta/2) \tag{4.11}$$

we obtain the relation between the impact parameter and the deflection angle which we are seeking:

$$b = \frac{k}{m v_0^2} \cot(\theta/2) . \tag{4.12}$$

In an actual experiment, we cannot measure the number of scattered particles arriving at a particular angle θ, but rather we have to consider the finite range of angles between θ and $\theta + d\theta$; these correspond to impact parameters in the range b to $b + db$. Then, by differentiating (4.12), we obtain the relation between db and $d\theta$:

$$db = -\frac{k}{2 m v_0^2} \frac{1}{\sin^2(\theta/2)} d\theta . \tag{4.13}$$

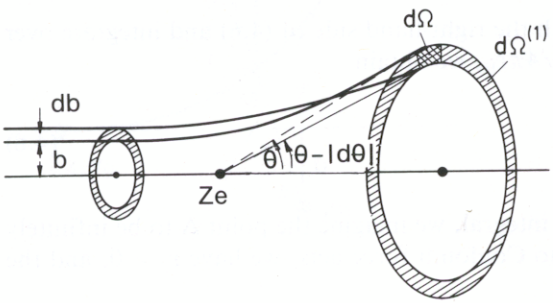

Fig. 4.8. Rutherford scattering. The incident alpha particles with impact parameters in the range b to $b + db$ are deflected into the range of angles θ to $\theta - |d\theta|$

Finally, we have to consider that the whole problem has rotational symmetry around an axis through the target nucleus and parallel to the direction of the incident beam (Fig. 4.8). Therefore, we have to consider a circular ring with radii $r_1 = b$ and $r_2 = b + db$, through which the incident beam enters and is scattered into the angular region from $\theta - |d\theta|$ to θ. [We note that with increasing impact parameter b the angle θ becomes smaller, see (4.12)]. This range of angles corresponds to an "effective area", the *differential cross section* da:

$$da = 2\pi b \, db . \tag{4.14}$$

If we shoot alpha particles through a thin foil with thickness D and area A, containing N atoms/cm^3, the "effective area" of all the atoms is

$$dA = 2\pi b db N D A \tag{4.15}$$

with the condition that the "effective areas" of the atoms do not overlap one another, which is a good assumption in a thin foil (up to 10000 atomic layers).

The probability that an incident alpha particle strikes the "effective area" of an atom in the foil is given by

$$W = \frac{\text{"effective area"}}{\text{total area}} = dA/A = 2\pi N D \, b \, db . \tag{4.16}$$

With a total of n alpha particles, the number dn' of the particles which strike the "effective area" and thus are deflected into the angle range θ to $\theta - |d\theta|$ is given by

$$dn' = n \cdot 2\pi N D\, b\, db\,. \tag{4.17}$$

These particles pass through the unit sphere around the target foil on a ring of area $d\Omega^{(1)} = 2\pi \sin\theta |\, d\theta\,|$. In the following, it is convenient to use the half-angle $\theta/2$; doing so, we obtain

$$d\Omega^{(1)} = 4\pi \sin(\theta/2)\cos(\theta/2)\,|\, d\theta\,|\,. \tag{4.18}$$

The detector which is used in the measurement cuts out a segment $d\Omega$ from this ring-shaped area. This surface element on the unit sphere is called a *solid angle*. The number of particles actually measured is therefore smaller than the number dn' by the ratio $d\Omega/d\Omega^{(1)}$. If the detector subtends a solid angle of $d\Omega$, the number of particles observed at angle θ is given by

$$dn = dn' \cdot d\Omega/d\Omega^{(1)}\,. \tag{4.19}$$

Inserting b and db from (4.12) and (4.13), we obtain the full Rutherford formula:

$$\frac{dn(\theta, d\theta)}{n} = \frac{Z^2 e^2 D N}{(4\pi\varepsilon_0)^2 m^2 v_0^4 \sin^4(\theta/2)}\, d\Omega \tag{4.20}$$

with n the number of incident particles, dn the number of particles scattered at an angle θ into the solid angle $d\Omega$, Z the (target) nuclear charge, e the elementary charge, D the target foil thickness, N the number of atoms/cm^3 in the target foil, $d\Omega$ the solid angle subtended by the alpha particle detector, ε_0 the permittivity constant of vacuum, m the mass of the scattered (alpha) particles, v_0 the velocity of the incident particles, and θ the angle of deflection.

This formula tells us how many particles dn out of the incident number n are scattered at a particular angle θ into a particular solid angle $d\Omega$, when target properties and incident particle velocity are known. Corresponding to (4.20), we find for the differential cross section (4.14)

$$da = \frac{Z^2 e^4}{(4\pi\varepsilon_0)^2 m^2 v_0^4 \sin^4(\theta/2)}\, d\Omega^{(1)}\,. \tag{4.21}$$

Furthermore, it is useful to define the *macroscopic (differential) cross section* $N da$, which is equivalent to the "effective area" dA per unit volume. By integration of (4.21) over $\Omega^{(1)}$, we can obtain the *total interaction cross section* a; the latter, however, diverges in the present case of a pure (unscreened) Coulomb potential, since (4.21) diverges for $\theta \to 0$. In the Rutherford scattering formula (4.20) for scattering by a foil, the limiting case $\theta \to 0$ is in principle not physically relevant: this is a result of the model, since $\theta = 0$ means that $b = \infty$. An infinite value of the impact parameter is, however, unreasonable given the assumed dense packing of the target atoms; the largest possible impact parameter is equal to half the distance between target atoms in the foil. For $\theta = \pi$, dn/n shows a minimum. This corresponds to $b = 0$. For very small impact parameters, there are deviations between the results of the calculation using the scattering formula (4.20) and the experiments. This occurs because the model of a deflection of the alpha particles by the Coulomb field of the nuclei alone is insufficient. From the

values of the impact parameter b for which these deviations become important, we can determine the nuclear radius R. This will be discussed in the following section.

4.2.4 Experimental Results

The Rutherford formula has been experimentally tested with great care. Keeping the solid angle $d\Omega$ constant, the $\sin^{-4}(\theta/2)$-law is found to be excellently reproduced in the counting rate (Fig. 4.5). Even with alpha particles of energy 5 MeV and scattering angles of 150°, no deviations from the Rutherford formula are found; this corresponds to an impact parameter of $6 \cdot 10^{-15}$ m. In this region, only the Coulomb potential of the nucleus has a measurable effect on the alpha particles.

The experimental tests of the Rutherford scattering formula can be summarised as follows:

The Coulomb law is obeyed well even at very small impact parameters, since the Rutherford formula is still valid. The nuclear radius is thus

$$R < 6 \cdot 10^{-15}\,\text{m}\,.$$

From experiments with different foil materials, the nuclear charge Z can be determined. The experiments of *Chadwick* (1920) verified that Z is identical with the position of the element in the periodic table.

The nucleus was originally assumed to be constructed from A protons and $(A-Z)$ electrons where A is the mass number defined on p. 6. After 1932 it was known that this model is not correct; $(A-Z)$ is rather the number of neutrons and Z is the number of protons in the nucleus.

We come now to the so-called *anomalous* Rutherford scattering. In the scattering of very fast alpha particles ($E > 6$ MeV) at large angles θ, i.e., with small impact parameters b – nearly central collisions – one observes clear *deviations* from the Rutherford formula. Here the Coulomb law is apparently no longer obeyed. The alpha particles approach the nuclei so closely that another, short-range interaction force becomes effective: the nuclear force. From the values b and θ at which deviations from the Rutherford formula, i.e., from the Coulomb law begin to occur, a nuclear size of $R \cong 10^{-15}$ m is obtained. This means that the density of the nucleus is about 10^{15} times larger than the density of the atom as a whole. These deviations from the scattering behaviour expected on the basis of the Rutherford formula are called *anomalous Rutherford scattering.*

The Rutherford model may be developed further. Negative electrons orbit around the positively charged nucleus with nuclear charge Z. This represents a dynamic equilibrium: without the motion of the electrons, no stability would be possible. If deflections of alpha particles through large angles are possible without causing a noticeable energy loss on the part of the alpha particles, then the mass of the target nucleus must be large compared to that of the alpha particle. On the other hand, observations with cloud chambers filled with helium gas, in which the target and the projectile, i.e., a He atom and an alpha particle, have virtually the same mass, show deflections of about 90°. From such experiments one can show that the nucleus must contain nearly the whole mass of the atom.

By contrast, momentum conservation requires that in a collision between an alpha particle and an electron, due to the small electron mass only very little momentum can be transferred. With the electron/alpha particle mass ratio, the deflection of the alpha particles can be no larger than 28″.

For very large impact parameters (small deflection angles), the Rutherford formula is likewise no longer exactly valid. The Coulomb potential of the nucleus is perturbed by the atomic electrons. These effects occur for $b \geqq 10^{-10}$ cm (deflection angles of a few seconds of arc) and are very difficult to detect experimentally. Completely analogous scattering formulae and scattering problems occur in the scattering of protons by atomic nuclei. The angular dependence of the scattering is related to the scattering potential; the latter can thus be determined from experiment. Scattering processes play an important rôle in nuclear and elementary particle physics, in the investigation of the internal structure of nuclei and of certain elementary particles. For example, *Hofstadter* was granted the Nobel Prize in 1961 for his scattering experiments using fast electrons (10^9 eV) on protons and neutrons. From the angular dependence of the scattering intensity, he was able to obtain information about the inner structure of the proton and of the neutron.

4.2.5 What is Meant by Nuclear Radius?

We can summarise our considerations in the above sections as follows: an alpha particle, which approaches a nucleus from outside the atom, is acted on at first only by the repulsive Coulomb potential. If it approaches the nucleus sufficiently closely, it will also be acted upon by the attractive nuclear force. The nuclear radius is defined as the distance at which the effect of the nuclear potential is comparable to that of the Coulomb potential (Fig. 4.9). For such investigations, alpha particles of high kinetic energies are used, so that they can approach the nucleus sufficiently closely.

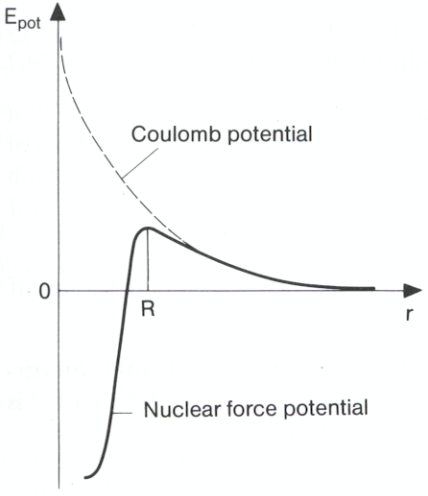

Fig. 4.9. Nuclear force and Coulomb potentials, used for defining the nuclear radius R

The empirical result of such measurements on nuclei with the mass number A is found to be

$$R = (1.3 \pm 0.1) A^{1/3} \cdot 10^{-15}\,\mathrm{m}\,.$$

Numerical examples for $A = 12$ and $A = 208$ are:

$$R(^{12}_{6}\mathrm{C}) = 2.7 \cdot 10^{-15}\,\mathrm{m}\,, \qquad R(^{208}_{82}\mathrm{Pb}) = 7.1 \cdot 10^{-15}\,\mathrm{m}\,.$$

This relationship between the nuclear mass and the nuclear radius implies that the density of nuclear matter is constant and independent of the size of the nucleus. This is one of the experimental results underlying the liquid-drop model for nuclei.

Problems

4.1 An aluminium foil scatters 10^3 α particles per second in a given direction and solid angle. How many α particles will be scattered per second in the same direction and solid angle if the aluminium foil is replaced by a gold foil of the same thickness?

4.2 The number of α particles scattered from a foil into a counter is $10^6\,s^{-1}$ for a scattering angle of 10°. Calculate from this the number of α particles which will be scattered into this counter as it is moved on a circular path from 10° to 180°. Show your results for $N(\theta)$ graphically.

4.3 Determine the distance of the closest approach of protons to gold nuclei in head-on collisions in which the protons have kinetic energies of (a) 10 MeV and (b) 80 MeV, and compare the results with the nuclear radius. In which case would the proton "touch" the nucleus? Determine the kinetic energy of the proton when it "touches" the nucleus.

4.4 Through what angle is a 4 MeV α particle scattered when it approaches a gold nucleus with a collision parameter of 2.6×10^{-13} m?

4.5 How large is the collision parameter of an α particle with 4 MeV kinetic energy which is scattered through the angle $\theta = 15°$ by collision with a gold nucleus ($Z = 79$)?

4.6 A beam of α particles with 12.75 MeV kinetic energy is scattered off a thin aluminium foil ($Z = 13$). It is observed that the number of particles which are scattered in a certain direction begins to deviate from the value calculated for pure Coulomb scattering at the deflection angle $\theta = 54°$. How large is the radius of the Al nucleus if one assumes that the α particle has a radius $R_\alpha = 2\times10^{-15}$ m?

Hint: Calculate the orbit according to (4.8 and 9) up to $\phi_0 = (180 - \theta)/2$, the point of closest approach, and determine $r(\phi_0)$.

4.7 A tight bunch of protons with uniform energy strikes a 4 μm thick gold foil perpendicular to the direction of flight. Of these protons, the fraction $\eta = 1.35\times10^{-3}$ is scattered through the angle $\theta = 60°$ in the angular interval $d\theta$.

a) What is the kinetic energy of the colliding protons?
b) Calculate the differential effective cross section $da(\theta)/d\Omega$ of the gold nucleus.
c) What is the collision parameter b?

Hint: Use (4.20) and the expression

$$\frac{dn/n}{d\Omega} = ND\frac{da(\theta)}{d\Omega}.$$

4.8 Why are α particles used for scattering from the gold atoms in the Rutherford experiment, and not electrons? What advantages and/or disadvantages would neutrons have as projectiles?

5. The Photon

5.1 Wave Character of Light

The fact that light can be regarded as a wave phenomenon was experimentally shown in the 17th and 18th centuries by the Dutch physicist *Huygens* and the English physician *Young* with the aid of interference experiments. In the 19th century, the physical nature of these waves came to light: they are electromagnetic waves, described by Maxwell's equations. They are characterised by the field vectors $\boldsymbol{E}$ and $\boldsymbol{B}$ of the electric and the magnetic field and exhibit a periodicity with the frequency ω.

In the year 1885, the theory of electromagnetic phenomena was completed with the formulation of the Maxwell equations. Two years later (1887), *Hertz* succeeded in demonstrating that such waves can be produced in the laboratory as emissions from an oscillating dipole. According to *Maxwell*, an electric and a magnetic field propagate away from an accelerated charge with the velocity of light. The accelerated charge radiates energy. The emission of light in the oscillator model is a result of a high frequency oscillation carried out by a charged particle. In absorption and in scattering of light, the incident electromagnetic wave excites the oscillator to forced oscillations. This classical Maxwell theory permits the precise calculation of the electromagnetic waves which are emitted by radio and radar antennas. Furthermore, it completely describes all of the wave properties of electromagnetic radiation, for example interference and diffraction.

Electromagnetic waves may be produced over an extremely wide range of frequencies (see Fig. 8.1); for this purpose, a number of different processes may be used.

Besides the oscillating dipole, some other examples are:

- the emission of light by the electrically charged particles in particle accelerators. Here, the *synchrotron radiation* is particularly noteworthy. The circulating particles in a circular electron accelerator emit radiation with a continuous spectrum. This radiation is utilised – for example at the German Electron Synchrotron (DESY) in Hamburg – as an intense, continuous, polarised light source for spectroscopy in the near, mid-, and far ultraviolet spectral regions. Figure 5.1 shows a schematic illustration of the accelerator in Hamburg. In Fig. 5.2, the spectrum of the synchrotron radiation is indicated. At relativistic particle energies, i.e., when the particle velocity is no longer small compared to the velocity of light, the emitted synchrotron radiation energy is a considerable fraction of the total energy which must be expended to operate the accelerator.

  Originally, electron synchrotrons were constructed as particle accelerators for high-energy physics research, and the synchrotron radiation was only a byproduct. Today, special storage rings ("dedicated sources") are built expressly for producing radiation, and yield intense beams of photons up to very high energies. An ex-

ample of such a large "third-generation" machine is the European Synchrotron Radiation Facility (ESRF) in Grenoble, France.

- A radiation emission which is produced in a similar manner and which is also called synchrotron radiation occurs when charged particles become trapped in the magnetic field of the earth. This phenomenon also occurs in distant regions of space, for example in the famous Crab nebula. Various astronomical objects are known to emit radiation in frequency regions from the far ultraviolet down to radio frequencies.
- A negative acceleration of electrons – for example a slowing down in the field of an atomic nucleus – leads to the emission of x-rays, the so-called bremsstrahlung.
- The thermal radiation of the sun is the energy source for all life on the earth.

While the wave character of light must be considered to be an experimentally and theoretically well-established fact, especially because of diffraction and interference phenomena, there are, on the other hand, experiments in which light behaves as particles; these are called *light quanta* or *photons.*

Before we describe the experiments which demonstrate the particle nature of light, we will summarise the most important physical properties of photons.

Photon

Energy	$h\nu$	Momentum	$p = h\nu/c = h/\lambda$
Velocity	c	Intrinsic angular momentum (spin)	$h/2\pi$
Rest mass	$m = 0$		

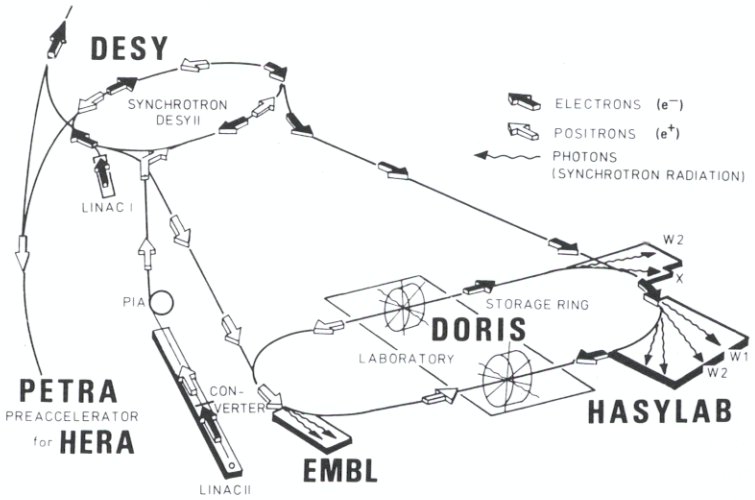

Fig. 5.1. A schematic representation of the electron synchrotron DESY and the storage ring DORIS in Hamburg. Electrons are preaccelerated by linear accelerators; positrons are generated in a converter target and stored in the accumulator storage ring PIA. Then both kinds of particles are further accelerated in the synchrotron DESY II and injected into the DORIS ring, where they can be stored for several hours. Alternatively, the particles may be accelerated to still higher energies in the former storage ring PETRA, and then injected into the electron-proton storage ring HERA (not shown in the drawing), where they are used for experiments in high-energy physics. The DORIS storage ring is used both for high-energy physics and as a large-scale source of photons for experiments with synchrotron radiation. In the facilities of the Hamburg Synchrotron Radiation Laboratory (HASYLAB) and the European Molecular Biology Laboratory (EMBL), about 30 experimental stations have been constructed for synchrotron radiation experiments. (Provided by C. Kunz, Hamburg University)

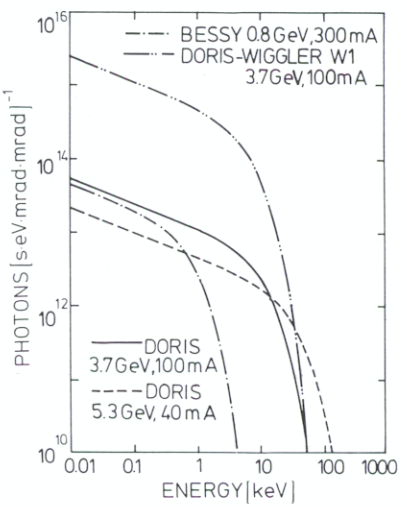

Fig. 5.2. The spectral intensity distribution of the synchrotron radiation from various electron synchrotrons and storage rings (photons/s eV mrad^{-2}). The radiation is continuous from the visible into the x-ray regions. In the far-ultraviolet and soft x-ray regions, an electron or positron storage ring is currently the best radiation source available. In addition to the spectrum emitted from the bending magnets of BESSY (in Berlin) and HASYLAB (in Hamburg), we show the considerably higher photon flux from the 32-pole "wiggler" W1 at HASYLAB. (Provided by C. Kunz, Hamburg University)

For converting from the quantum energy of a photon $E = h\nu$, which is often expressed in eV, to the vacuum wavelength λ_{vac} of the light wave, the following relation holds:

$$E\,[\text{eV}] = 12398/\lambda\,[\text{Å}]\,. \tag{5.1}$$

In the next sections we will describe three experiments which can only be understood by assuming the existence of photons.

5.2 Thermal Radiation

5.2.1 Spectral Distribution of Black Body Radiation

The quantisation of energy in the interaction of light with matter was postulated for the first time by *Planck* in the year 1900 in his theoretical analysis of the spectral distribution of the light emitted by a black body radiator (defined below), which had been experimentally determined. This light is referred to as thermal or black body radiation.

Hot objects emit light radiation as a result of their temperature. This is an everyday experience. It is well known that the colour which we see in a thermal radiator (for example a furnace) changes from dark red to bright red to yellow to white as the temperature of the furnace is increased. The determination of the colour in the interior of a furnace is used as a measure of its temperature; this technical application is called *pyrometry*.

At temperatures below a few hundred kelvins, the radiation emitted is for the most part infrared light, also called heat radiation. This infrared radiation is responsible for the fact that a thermally isolated object eventually reaches the same temperature as its surroundings. If one wishes to carry out experiments at very low temperatures (e.g., 4.2 K and below), the experimental region must therefore be screened from the thermal radiation of the laboratory, which is at room temperature, by using cooled thermal shields.

The laws governing the spectral intensity distribution of thermal radiation are obtained by the experimental analysis of the *black body radiator*. This is a cavity which emits radiation being in thermal equilibrium with its walls; the material of the walls emits and absorbs thermal radiation.

Experimentally, a source of black body radiation is most easily obtained by making a small hole in the wall of a cavity which is held at constant temperature. The hole is so small that neither the radiation which enters the cavity from outside, nor that which escapes to the outside, is sufficient to alter the thermal equilibrium in the cavity (Fig. 5.3). The energy density $u(\nu, T)$ of the radiation field within the cavity can be determined by measuring the radiative power (energy per unit time) $N(\nu, T)$ connected with the spectral radiative flux density $P(\nu, T)$ which passes out of the hole, using a spectrometer. The spectral energy density $u(\nu, T)$ is defined as

$$u(\nu, T)\,d\nu = \frac{\text{radiation energy in the frequency range } \nu \ldots \nu + d\nu}{\text{volume}}$$

and the spectral radiative flux density $2P(\nu, T)$ as

$$2P(\nu, T)\,d\nu = \frac{\text{radiative power in the frequency range } \nu \ldots \nu + d\nu}{\text{area} \cdot \text{solid angle}}\,.$$

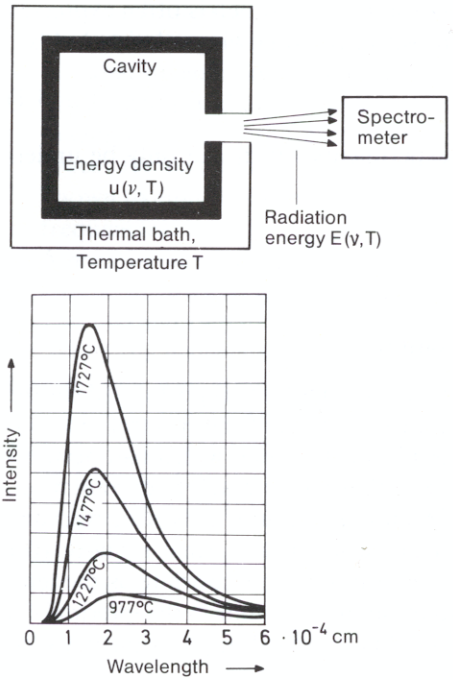

Fig. 5.3. Thermal radiation. *Upper part:* Schematic illustration of a cavity radiator. *Lower part:* Typical measured curves of the intensity distribution in the black body radiation at various temperatures

$2P(\nu, T)\,d\nu$ is the quantity of energy within the frequency interval $\nu \ldots \nu + d\nu$ which is radiated per unit time through a unit area into the solid angle 1 sterad normal to the surface. The factor 2 in the definition comes from the fact that the radiation can be decomposed into two components with polarisation directions perpendicular to each other. $P(\nu, T)\,d\nu$ for one component, i.e., for linearly polarised radiation, is independent of the polarisation direction for a black body radiator. For the energy radiated from a surface A at an angle θ to the surface normal as unpolarized radiation into the solid angle $\Delta\Omega$, we have (in the time interval Δt and the frequency range $\nu \ldots \nu + d\nu$):

$$E = u(\nu, T)\,d\nu \cdot c \cdot \Delta t \cdot (\Delta\Omega/4\pi) A \cos\theta \ . \tag{5.2}$$

Figure 5.3 shows some typical experimental results. The radiation has a continuous spectrum with a prominent maximum, which lies in the infrared when the black body radiator is at room temperature.

The following results are important:

– At a given temperature, the energy distribution is the same, independently of the shape and material of the cavity.

In (5.2), the radiation in a frequency interval from ν to $\nu + d\nu$ at an angle θ is calculated. The radiated power of the surface element per polarization direction in all directions into a hemisphere can be found by integration over angles:

$$P(\nu, T)_{\text{tot}} = \frac{c}{8\pi} u(\nu, T) \int_0^{2\pi} d\phi \int_0^{\pi/2} \cos\theta \sin\theta \, d\theta = \frac{c}{8} u(\nu, T) \ . \tag{5.2a}$$

The limits of integration here imply that the surface can only radiate outwards (into a hemisphere, see Fig. 5.3). From this expression we obtain the total radiation at a temperature T by integrating over all frequencies and polarization directions:

$$S = 2 \int_0^\infty P(\nu, T)_{\text{tot}}\, d\nu = \sigma \cdot T^4 \ . \tag{5.3}$$

This is the Stefan-Boltzmann Law, with $\sigma = 5.670 \cdot 10^{-8}\ \text{Wm}^{-2}\,\text{K}^{-4}$.

– The Wien Displacement Law holds for the wavelength at which the maximum intensity $\lambda_{\max}$ occurs in the emitted spectrum, as a function of temperature:

$$\lambda_{\max} T = \text{const} = 0.29\ \text{cm K} \ . \tag{5.4}$$

As an example we can take the solar radiation: the surface temperature of the sun is 6000 K; the wavelength at maximum intensity is $\lambda_{\max} = 480$ nm.

– The law derived by *Rayleigh* and *Jeans* from classical electrodynamics,

$$P = \frac{\nu^2}{c^2} kT \tag{5.5}$$

describes the radiative flux density per polarisation direction very well for *low* frequencies. However, at *high* frequencies, this law cannot be correct: if it is integrated over all frequencies, it yields an infinitely large energy density – we encounter the so-called ultraviolet catastrophe. Within classical electrodynamics and thermodynamics it was not possible to find an expression for P which agreed with experiment at high frequencies. This was accomplished for the first time by the Planck formula.

5.2.2 Planck's Radiation Formula

According to *Planck*, the experimentally determined spectral energy density of the radiation per unit volume, in the frequency interval $\nu \ldots \nu + d\nu$, can be represented by

$$u(\nu, T)\, d\nu = \frac{8\pi h \nu^3}{c^3} \frac{1}{e^{h\nu/kT} - 1} d\nu \ . \tag{5.6}$$

From this we obtain for the radiative flux density per polarisation direction and solid angle

$$P(\nu, T)\, d\nu = \frac{h\nu^3}{c^2 (e^{h\nu/kT} - 1)} d\nu \ .$$

These radiation formulae may be derived by making the following assumptions:

1) The atoms in the walls of the cavity behave like small electromagnetic oscillators, with each having its characteristic oscillation frequency ν. They radiate electromagnetic radiation out into the cavity and absorb radiation from the cavity; a thermal equilibrium is established between the radiation in the cavity and the atoms in the cavity walls. The excitation of the oscillators depends on the temperature.
2) The oscillators cannot – like classical oscillators – take on all possible values of energy, but rather only discrete values described by

$$E_n = n \cdot h \cdot \nu \ , \tag{5.7}$$

where n is an integer $n = 0, 1, 2, \ldots$ and h is Planck's constant ($h = 6.626176 \cdot 10^{-34}$ Js $= 4.14 \cdot 10^{-15}$ eVs). Today we know that this *quantisation* is more correctly described by the equation

$$E_n = (n+1/2)\,h\nu\,. \tag{5.8}$$

The quantity $h\nu/2$ is the *zero-point energy* of the oscillator. We will derive (5.8) using a quantum mechanical treatment in Chap. 9.

3) As long as the oscillator is not emitting or absorbing (radiation) energy, it remains in its quantum state, characterised by the quantum number n.
4) The number of possible states of oscillation of the electromagnetic field in the cavity of volume V between ν and $\nu+d\nu$ for both polarisation directions is given by

$$dZ = \frac{8\pi V\nu^2}{c^3}\,d\nu\,, \tag{5.9}$$

which can be derived in classical electrodynamics.

The existence of discrete energy values represents a contradiction to the experience of classical physics, where energy always seems to occur with continuous values. The reason that quantised energy steps are not observed in classical physics is the smallness of the Planck constant h. We give a numerical example to make this clear:

A mass-and-spring harmonic oscillator with a mass $m = 1$ kg and a spring constant $f = 20\ \mathrm{Nm}^{-1}$ is oscillating with an amplitude $x_0 = 10^{-2}$ m. Its characteristic frequency is then given by

$$\nu = (1/2\pi)\sqrt{f/m} = 0.71\ \mathrm{s}^{-1}\,.$$

The energy of the oscillator is

$$E = fx_0^2/2 = 1.0\cdot 10^{-3}\ \mathrm{J}\,.$$

This energy corresponds to n energy quanta of the frequency ν:

$$n = E/h\nu = \frac{10^{-3}\ \mathrm{J}}{6.6\cdot 10^{-34}\ \mathrm{Js}\cdot 0.7\ \mathrm{s}^{-1}} = 2.1\cdot 10^{30}\,.$$

If n now changes to $n\pm 1$, this produces a relatively energy change of

$$\Delta E/E = \frac{h\nu}{n\cdot h\nu} \cong 10^{-30}\,.$$

The relative change is thus extremely small.

From this we conclude that an energy quantisation for macroscopic systems in the realm of classical physics cannot be detected, due to the extremely large quantum numbers which occur.

5.2.3 Einstein's Derivation of Planck's Formula

The derivation of the Planck radiation formula due to *Einstein* (1917) is an interesting example of the combination of optics, thermodynamics, and statistics. *Einstein* assumed that light consists of particles, the so-called light quanta or photons. Each

light wave of frequency ν corresponds to a number of photons. Furthermore, in this theory the existence of discrete atomic energy levels is already assumed. The justification for this latter assumption in terms of the Bohr atomic model will be treated in Chaps. 8 and 9; we thus anticipate it here.

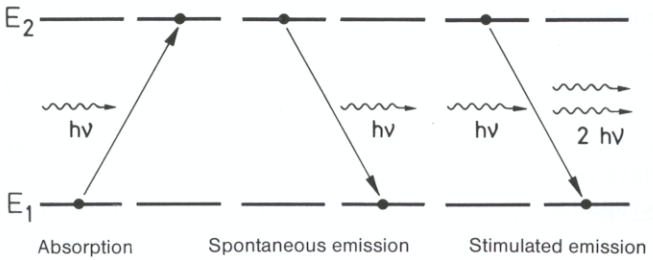

Fig. 5.4. Absorption, spontaneous and stimulated emission of radiation with the quantum energy $h\nu$ between two energy levels E_1 and E_2

An atom with two energy levels E_1, E_2 may, according to *Einstein*, interact with electromagnetic radiation in three different ways:

- *Absorption* of a light quantum takes the atom from the lower level E_1 into the energetically higher level E_2. In the process, a light quantum of energy $\Delta E = E_2 - E_1 = h\nu$ is removed from the radiation field.
- *Emission* occurs from the level E_2 *spontaneously* within a time known as the mean lifetime. A light quantum of energy ΔE is thereby released into the radiation field.
- Just as light quanta can be absorbed, light quanta in the radiation field can also stimulate the emission of further quanta when the atom is in the higher level E_2. For this stimulated or *induced emission*, primary light quanta are thus necessary. Another light quantum joins those which were already present in the radiation field.

These processes are shown schematically in Fig. 5.4.

In order to derive *Planck*'s formula, we consider, following *Einstein*, a system of N atoms. The numbers of atoms in the level E_1 or E_2 are denoted by N_1 and N_2, respectively. The system is taken to be in thermal equilibrium with its surroundings. Interactions with the radiation field are only possible in the form of emission or absorption of radiation as discrete energy quanta $h\nu = E_2 - E_1$.

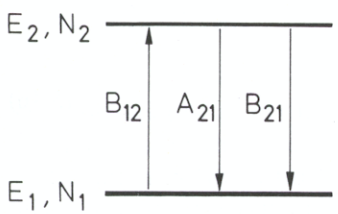

Fig. 5.5. Derivation of the Planck formula: two energy levels E_1 and E_2 with occupation numbers N_1 and N_2 are connected by transitions with the probabilities B_{12}, B_{21} and A_{21}

The radiation field is taken to have the radiation energy density $u(\nu, T)$, which we will denote in the following simply as $u(\nu)$. It then produces, per unit time, the following transitions (Fig. 5.5):

Absorption from 1 to 2. The number of processes in time dt is proportional to the occupation number N_1 of level 1 and to the radiation energy density $u(\nu)$:

$$dN_{12} = B_{12} u(\nu) N_1 dt \,. \tag{5.10}$$

The proportionality constant B_{12} is called the Einstein coefficient and is a measure of the transition probability per unit time and radiation density.
Transitions from 2 to 1 are composed of two contributions, as seen in Fig. 5.5: the first is *spontaneous emission from 2 to 1.* The number of such processes per unit time is proportional to the occupation number N_2. We have:

$$dN'_{21} = A_{21} N_2 dt \,. \tag{5.11}$$

A_{21} is also an Einstein coefficient and is a measure for the transition probability per unit time. Furthermore, we have *induced emission from 2 to 1.* It is, analogously to (5.10), proportional to the occupation number N_2 and to the radiation density $u(\nu)$. The result is:

$$dN''_{21} = B_{21} u(\nu) N_2 dt \,. \tag{5.12}$$

B_{21} is defined in an analogous way to the Einstein coefficient B_{12} in (5.10).

In equilibrium, an equal number of transitions occurs in each direction. We must therefore have

$$dN_{12} = dN'_{21} + dN''_{21} \,. \tag{5.13}$$

Setting (5.10) and (5.11, 12) equal leads to the following ratio of the occupation numbers:

$$N_2/N_1 = \frac{B_{12} u(\nu)}{A_{21} + B_{21} u(\nu)} \,. \tag{5.14}$$

Since the system is in thermal equilibrium, the ratio of the occupation numbers of the two energy levels can also be calculated according to the Boltzmann distribution. It must then be true that

$$N_2/N_1 = \mathrm{e}^{-E_2/kT} / \mathrm{e}^{-E_1/kT} \,. \tag{5.15}$$

From these two equations follows

$$\frac{B_{12} u(\nu)}{A_{21} + B_{21} u(\nu)} = \mathrm{e}^{-E_2/kT} / \mathrm{e}^{-E_1/kT} \tag{5.16}$$

and

$$u(\nu) = \frac{A_{21}}{B_{12} \mathrm{e}^{h\nu/kT} - B_{21}} \tag{5.17}$$

with the abbreviation $E_2 - E_1 = h\nu$.

To determine the coefficients A and B, we use the limiting condition that $u(\nu)$ must go to infinity when $T \to \infty$, i.e., the denominator of (5.17) must go to zero. Then we have

$$B_{12} = B_{21} \,. \tag{5.18}$$

From this follows

$$u(\nu) = \frac{A_{21}}{B_{12}(e^{h\nu/kT} - 1)} . \tag{5.19}$$

Furthermore, the experimentally verified Rayleigh-Jeans law must hold for small frequencies, i.e., for $h\nu \ll kT$, see (5.5),

$$u(\nu) = \frac{8\pi\nu^2 kT}{c^3} . \tag{5.20}$$

For small values of the exponent $(h\nu/kT)$ we can use a series expansion for the exponential function: $\exp(h\nu/kT) = 1 + h\nu/kT + \ldots$. Inserting this in (5.19) yields

$$u(\nu) = \frac{A_{21}}{B_{12}} \frac{kT}{h\nu} \quad (\text{for } h\nu \ll kT) , \tag{5.21}$$

which, combining with the Rayleigh-Jeans law (5.20), leads to

$$\frac{A_{21}}{B_{12}} = \frac{8\pi h\nu^3}{c^3} \quad (\text{holds generally}) . \tag{5.22}$$

Finally, inserting in (5.19),

$$u(\nu) = \frac{8\pi h\nu^3}{c^3} \frac{1}{e^{h\nu/kT} - 1} . \tag{5.23}$$

Equation (5.23) is the Planck formula.

Rearranging (5.22), we find for the relation between the Einstein coefficients for transitions between levels 2 and 1,

$$A_{21} = \frac{8\pi h\nu^3}{c^3} B_{12} . \tag{5.24}$$

This corresponds to the Kirchhoff relation, according to which the probabilities for spontaneous emission and absorption are proportional.

Equation (5.18) is, furthermore, an expression of the fact that the radiation field takes up and gives out radiation quanta in like fashion; absorption and stimulated emission are fully complementary physical processes.

Einstein's derivation of the Planck formula lends strong support to the existence of light quanta of energy $h\nu$. From the equation $E = h\nu$ and the equivalence of mass and energy, $E = mc^2$, it follows that a mass can also be ascribed to the photon, having the value $m_{ph} = h\nu/c^2$. However, the rest mass of the photon is in fact zero.

5.3 The Photoelectric Effect

In the year 1888, *Hallwachs* measured for the first time the laws governing the release of electrons from metals by light, the *photoelectric effect*, following earlier observations by *Hertz*. The results of his experiments were explained in 1905 by *Einstein* using the hypothesis of light quanta.

The photoeffect may be simply demonstrated, qualitatively, using the setup shown in Fig. 5.6. A zinc plate is activated on its surface by rubbing with mercury and is mounted in an electrically insulated holder. If it is negatively charged and then illuminated with ultraviolet light, it rapidly discharges. A positively charged plate cannot be discharged by light.

From these experiments we see that light sets electrons from the plate free. The negatively charged plate releases these electrons to the surrounding air; the positively charged plate retains them due to Coulomb attraction. These experiments may be made more quantitative by replacing the electrometer with a so-called dropping electrometer; the quantity of charge released from the plate can then be measured as a function of the intensity and energy of the light.

If one also wishes to measure the kinetic energy of the electrons, the counter-field method may be used: one measures the maximum voltage V_{max} which is just sufficient

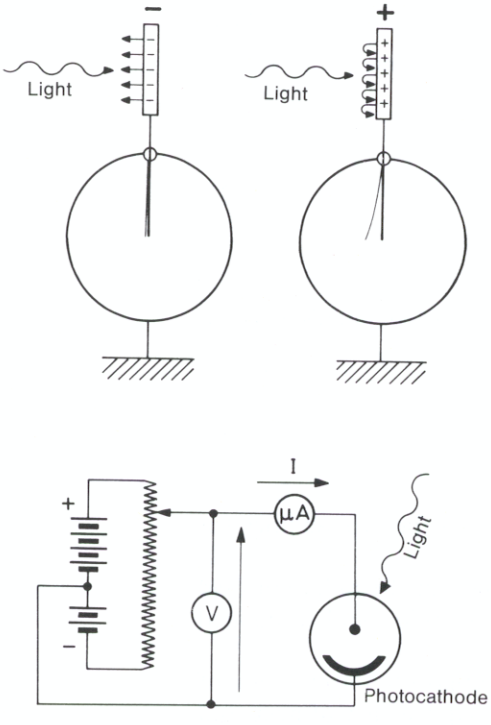

Fig. 5.6. Photoeffect. *Upper part:* A negatively charged electrometer is discharged upon illumination of the electrode, a positively charged one is not. *Lower part:* Arrangement for quantitative study of the photoeffect (voltage V, current I)

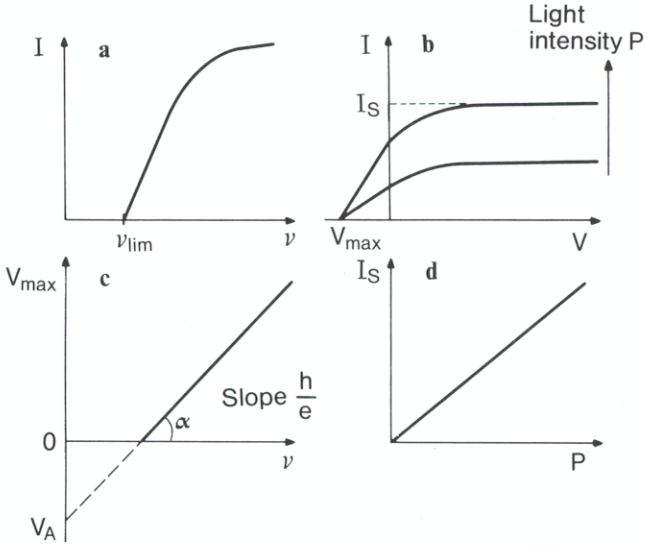

Fig. 5.7a – d. Quantitative results for the photoeffect. **a)** Photocurrent I as a function of the frequency ν of the light. Below the limiting frequency ν_{lim} there is no longer a photocurrent. **b)** Photocurrent I as a function of the applied voltage V. Positive values of the voltage here mean that the irradiated electrode is the *cathode*. The largest negative voltage which can still be overcome by the photoelectrons (when the irradiated electrode is the *anode*) is V_{max}. The saturation current I_S is a function of the light intensity P. **c)** Maximum braking voltage V_{max} as a function of the light frequency ν; measurement of the ratio h/e and of the work function V_A as the slope and intercept of the straight line according to (5.28). It should be remembered that in the counter-field method, both work functions, that of the cathode and that of the anode, are to be taken into account. **d)** Saturation current I_S as a function of the light intensity P. The current increases with the intensity

to keep the electrons from leaving the plate. For this purpose, the setup shown in the lower part of Fig. 5.6 may be used, with the illuminated electrode however attached to the *positive* pole of the voltage source.

The results of such an experiment are shown in Fig. 5.7: the electron current I as a function of the frequency ν of the light begins at a limiting frequency ν_{lim} which is characteristic for the electrode material (Fig. 5.7a). The maximum kinetic energy of the electrons follows from the current-voltage characteristic curve of the apparatus (Fig. 5.7b). If the counter voltage – the braking potential – reaches a certain value V_{max}, dependent on the frequency of the light, the photocurrent drops to zero and remains so. The electrons which are emitted no longer have sufficient energy to overcome the braking potential. The expression $eV_{\text{max}} = mv^2/2$ gives the velocity of the electrons. If the maximum braking potential V_{max} is plotted against the frequency of the light, a straight line is found (Fig. 5.7c).

To understand these experiments, we need the *light quantum* hypothesis. Classically, it would be expected that the electric field E of the light, which is proportional to the square root of the light intensity, is responsible for the acceleration and release of the electrons from the electrode. The energy of the photoelectrons should increase with increasing light intensity. We find, however, that the energy of the photoelectrons does not depend on the light intensity (and thus on the radiation power), but only on the frequency of the light.

On the other hand, the number N of emitted electrons is proportional to the intensity P of the light (Fig. 5.7d).

Photoelectrons are only emitted when the light frequency is larger than a characteristic value ν_{lim} which depends on the electrode material. The following relation must hold:

$$h\nu \geqq h\nu_{\text{lim}} = eV_{\text{A}} . \tag{5.25}$$

Clearly, a part of the light energy $h\nu$ is used to release an electron from the metal electrode. For this purpose an amount of energy equal to eV_{A}, called the work function, is required. This work function is specific for the electrode material. The remainder of the energy of the light quantum is available to the electron as kinetic energy. The total energy of the light quantum is thus transferred in an elementary process to the electron. The energy balance is given by

$$\begin{array}{llll} mv^2/2 & = h\nu & - eV_{\text{A}} . & (5.26) \\ \text{kinetic energy of the photoelectron} & = \text{quantum energy of the light} & - \text{work function of the photoelectron} & \end{array}$$

The kinetic energy of the photoelectrons is equal to the energy eV_{max}; thus we can write (5.26) in the form

$$eV_{\text{max}} = h\nu - eV_{\text{A}} \tag{5.27}$$

or

$$V_{\text{max}} = h\nu/e - V_{\text{A}} . \tag{5.28}$$

The slope of the straight line which is obtained by plotting V_{max} against the frequency ν of the exciting light (Fig. 5.7c) can be used for a precision measurement of the ratio h/e. For the angle α of the slope we have

$$\tan \alpha = h/e \,. \tag{5.29}$$

Table 5.1 gives some examples for the work functions of various metals. The alkali metals are notable for their especially small work functions.

Table 5.1. Work functions eV_A and limiting wavelengths λ_{lim} of several metals

Metal	eV_A [eV]	λ_{lim} [nm]
Li	2.46	504
Na	2.28	543
K	2.25	551
Rb	2.13	582
Cs	1.94	639
Cu	4.48	277
Pt	5.36	231

An arrangement in which the electrons released from an electrode (photocathode) complete a circuit, open in the absence of light, between the photocathode and another electrode is called a *photocell.* Photocells are used in numerous applications in measurement and control technology.

Apart from the so-called external photoeffect, which we have discussed above, the same phenomenon is met again in many other areas of physics. In solid state physics, the release of normally bound charge carriers by the action of light is called the *internal photoeffect.* In this case, an increase in the electrical conductivity of semiconductors or insulators upon illumination may be observed. In nuclear physics, atomic nuclei can be excited and caused to emit nucleons, i.e., the particles of which the nucleus is composed, upon absorption of very short wavelength radiation (x-rays or gamma rays). This is termed the *nuclear photoeffect.*

5.4 The Compton Effect

5.4.1 Experiments

The Compton effect is the name given to the scattering of light by weakly bound or free electrons. This effect occurs in particular in the x-ray region of the electromagnetic spectrum. The incident light wave (x-radiation) excites electrons in the target atoms so that they oscillate. The oscillating electrons in the field of the positively charged nuclei may be considered as classical oscillators; they emit radiation themselves, with the same frequency as that with which they are driven. This radiation is called Rayleigh-scattered radiation. The theory of Rayleigh scattering was first developed for visible light; it explains the blue colour of the sky. Light of short wavelength (blue) is more strongly scattered than light of long wavelength (red light). The scattered radiation has the same wavelength as the primary radiation, and is polarised. In 1909 it was shown by *Barkla* that this type of scattering also occurs with x-radiation.

In 1921, *Compton* observed that in addition to the spectrally unshifted scattered radiation, a spectrally displaced component appeared (Fig. 5.8). There is a simple

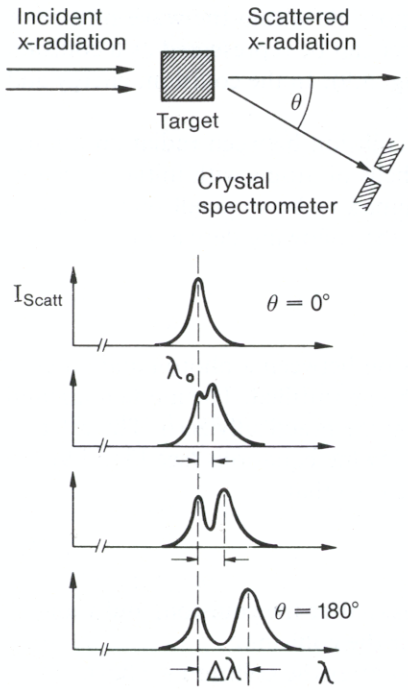

Fig. 5.8. Compton Effect. *Upper part:* Experimental setup. The x-radiation which is scattered by the target (e.g., a graphite block) is measured as a function of the scattering angle θ, which is defined to be 0° for undeflected radiation and 180° for radiation reflected back towards the source. *Lower part:* Measured scattered radiation as a function of wavelength for various scattering angles. The unshifted Rayleigh-scattered radiation as well as the shifted Compton-scattered radiation are seen

relation between the shift in the wavelength and the scattering angle: independently of the target material, it is found that

$$\Delta\lambda = \lambda_c(1 - \cos\theta) \tag{5.30}$$

with the *Compton wavelength* $\lambda_c = 0.024$ Å. The wavelength shift $\Delta\lambda$ is also completely independent of the primary wavelength. Only the *intensity* of the Compton scattering depends on the target material: it is especially large for light materials (Z small), as compared to the x-ray absorption which increases approximately with Z^3 (18.5).

Two numerical examples may serve to illustrate Compton scattering; the wavelength shift is a maximum at $\theta = 180°$. At an energy of 1000 eV for the light quanta before scattering, the energy of the 180°-scattered radiation is 996 eV; at a primary energy of 1 MeV, the 180°-scattered radiation has an energy 200 keV. In the former case, the energy is reduced by 4 eV or 0.4%, in the latter by 800 keV or 80%. In both cases, the corresponding shift in the *wavelength* is about $\Delta\lambda = 0.050$ Å.

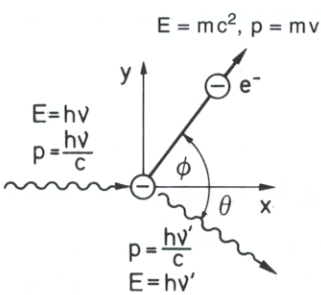

Fig. 5.9. Explanation of the Compton effect: the incident x-ray quantum with energy $E = h\nu$ and momentum $p = h\nu/c$ collides with an electron. In the collision, it transfers energy and momentum to the electron; the scattered x-ray quantum thus has a reduced energy $h\nu'$ and a reduced momentum $h\nu'/c$

The explanation of these experiments was not possible within the wave picture of light. Using the hypothesis of light quanta, the effect can be represented as a collision between two particles, a photon and an electron (Fig. 5.9). In the collision, energy and momentum are transferred.

More precisely, we are dealing with an elastic collision between radiation quanta and electrons that are weakly bound in the outer shells of atoms with initial velocities $v_0 \cong 0$. The binding energy of the electrons is assumed to be so small that it can be neglected in comparison with the photon energy in the following derivation.

5.4.2 Derivation of the Compton Shift

We consider the Compton effect as an elastic collision between a photon and an electron. Energy and momentum conservation must both be fulfilled. The momentum and the kinetic energy of the electron before the collision are practically zero. The calculation must be done relativistically, leading to the following equations (see Fig. 5.9).

Energy before and after the collision is conserved, so that

$$h\nu + m_0 c^2 = h\nu' + mc^2 . \tag{5.31}$$

Here m_0 is the rest mass of the electron and m its mass after the collision, and ν and ν' are the frequencies of the radiation before and after the collision.

For the momentum in the y direction before and after the collision we have

$$0 = \frac{h\nu'}{c} \sin\theta - mv \sin\phi \tag{5.32}$$

and for the momentum in the x direction

$$\frac{h\nu}{c} = \frac{h\nu'}{c} \cos\theta + mv \cos\phi . \tag{5.33}$$

In (5.31), we move $h\nu'$ to the left side and abbreviate $\nu - \nu' = \Delta\nu$. We then express the mass of the moving electron in terms of the rest mass, using the relativistic mass formula $m = m_0(1 - v^2/c^2)^{-1/2}$. If we now square (5.31) and rearrange somewhat, we obtain

$$h^2(\Delta\nu)^2 + 2m_0 c^2 h\Delta\nu = m_0^2 c^4 \frac{v^2}{c^2 - v^2} . \tag{5.34}$$

In order to eliminate the angle ϕ from (5.32) and (5.33), we solve these equations for $\sin\phi$ and $\cos\phi$ and use the identity $\sin^2\phi + \cos^2\phi = 1$. When we rearrange, we obtain

$$h^2[(\Delta\nu)^2 + 2\nu(\nu - \Delta\nu)(1 - \cos\theta)] = m_0^2 c^4 \frac{v^2}{c^2 - v^2} . \tag{5.35}$$

Since the right-hand sides of (5.34) and (5.35) are identical, we can set the left-hand sides equal to one another, obtaining

$$m_0 c^2 h\Delta\nu = h^2\nu(\nu - \Delta\nu)(1 - \cos\theta) . \tag{5.36}$$

We wish to express the result in terms of wavelengths instead of frequencies. Using $c = \lambda \nu$, we obtain

$$|\Delta\lambda| = \left|\frac{c}{\nu} - \frac{c}{\nu - \Delta\nu}\right| = \frac{c\Delta\nu}{\nu(\nu - \Delta\nu)} . \tag{5.37}$$

Inserting (5.37) into (5.36), we have finally

$$|\Delta\lambda| = \frac{h}{m_0 c}(1 - \cos\theta) = \lambda_c(1 - \cos\theta) , \tag{5.38}$$

where we have introduced the abbreviation $\lambda_c = h(m_0 c)^{-1}$ (the "Compton wavelength"). Incidentally, the quantum energy of radiation which has the Compton wavelength λ_c is just equal to the rest energy of an electron:

$$h\nu = hc/\lambda_c = m_0 c^2 = 511 \text{ keV} . \tag{5.39}$$

The energy and momentum of the recoil electrons may also be calculated with these equations. The energy received by the electrons is relatively small, but their paths can still be seen in a cloud chamber and be quantitatively determined. This was shown in 1925 by *Compton* and *Simon*.

Another experiment done by *Bothe* and *Geiger* in 1925 shows that the electrons and the photons are, in fact, "emitted" simultaneously in the Compton effect (Fig. 5.10). A scattering target is set up in the centre between symmetrically placed electron and photon detectors. The number of simultaneous counts in the two detectors is measured with a coincidence circuit, with the result that the number of coincidences observed is far greater than the number which would be expected by chance from uncorrelated events.

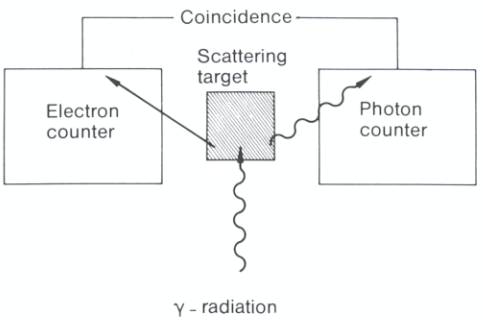

Fig. 5.10. Apparatus to detect coincidences between scattered x-ray quanta and recoil electrons from the Compton effect

The following remarks may be useful for a deeper understanding of the Compton effect:

- Compton scattering is relatively weak in the case of strongly bound electrons, that is in heavy atoms. When the electron's binding energy is large compared to the quantum energy $h\nu$ of the photon, no momentum transfer is possible.

- In certain energy ranges – in particular for medium-hard x-rays – the Compton effect is the principal cause of scattering and attenuation of radiation in matter.
- In Compton scattering, the incident and the scattered radiation are *incoherent* relative to one another (if $h\nu \neq h\nu'$).

We see that the photoeffect and the Compton effect can only be understood by assuming that light (radiation) consists of individual particles with a momentum p. On the other hand, we know from interference and diffraction experiments that light behaves as a wave, characterised by a wavelength λ and a frequency ν. The particle aspects of light which we summarised at the beginning of this chapter find their confirmation in the photoelectric and Compton effects.

How can we reconcile the wave and the particle character of the same phenomenon? To clarify this question we imagine the following experiment (Fig. 7.5): we allow a beam of light to pass through a small hole in an opaque wall and to fall on a screen. On this screen we observe, following the laws of wave optics, a diffraction pattern. We could, however, detect the light falling on the screen by means of the photoeffect or the Compton effect. If we now make the intensity of the light weaker and weaker, we find, using the photoeffect as detector, that locally, at particular points, single photoelectrons are set free by the light. The particle character of the radiation is here predominant. If this experiment is now repeated a number of times and the relative abundance of photoelectron releases is kept track of as a function of position, a distribution curve will be obtained which is in exact agreement with the diffraction pattern.

This thought experiment, which could actually be carried out as a real experiment, gives us the key to explaining the nature of light. Light carries – virtually, so to speak – both properties – wave and particle – within itself. Depending on the experiment we carry out, it shows us the one or the other aspect of its character. In order to combine both aspects, which at first appear contradictory, we have to apply statistical considerations. Thus in the case just described, if we perform an experiment which is intended to detect the diffraction pattern, but then inquire about the particle character, we find that we cannot predict the point at which the light particle will strike the screen with certainty. Instead, we can only give the probability that it will arrive at a particular point. The resulting probability distribution is then identical with the diffraction pattern which we would calculate according to the laws of classical physics. This statistical way of considering things is, as we shall see again and again, fundamental to the quantum mechanical interpretation of physical phenomena (Chap. 7.2).

Problems

5.1 Express the relativistic mass of a photon in terms of h, λ and c.

5.2 What is the momentum of a photon with 1 eV energy? Give the corresponding wavelength in Ångstroms.

5.3 How much mass does a 100 W light bulb lose in one year due to light emission?

5.4 A photon with 2 MeV of energy is converted into a positron-electron pair. What is the kinetic energy of the positron and electron, if the energy is equally distributed

between the two particles and the electrostatic interaction between the two is ignored? ($m_{e^-} = m_{e^+} \triangleq 0.511$ MeV). How large is their velocity?

5.5 In the upper atmosphere, molecular oxygen is split into two oxygen atoms by photons from the sun. The longest wavelength of photons which can do this have $\lambda = 1.75 \times 10^{-7}$ m. What is the binding energy of O_2?

5.6 A person can perceive yellow light with the naked eye when the power being delivered to the retina is 1.8×10^{-18} W. The wavelength of yellow light is about 6000 Å. At this power, how many photons fall on the retina each second?

5.7 A monochromatic beam of electromagnetic radiation has an intensity of 1 W/m^2. What is the average number N of photons per m^2 and second for a) 1 kHz radio waves and b) 10 MeV gamma rays?

5.8 Calculate the radiation pressure of sunlight when the incoming energy/(s m^2) is 1.4×10^3 W/m^2 and the radiation is completely absorbed. Compare this value with the atmospheric pressure. What is the force on a surface of 1 m^2? What is the force if the light is completely reflected?

Hint: The radiation pressure is the momentum transferred per unit of time and surface area.

5.9 A photon which is emitted by an atom imparts an equal and opposite momentum to the atom.

a) What is the kinetic energy transferred to the atom if the frequency of the photon is ν and the mass of the atom is M?
b) How much energy is transferred to the Hg atom in the emission of the mercury spectral line $\lambda = 2357$ Å? ($M_{Hg} \approx 200.6$ u).
c) What is the corresponding reaction energy in the emission of γ quanta with 1.33 MeV energy by ^{60}Ni? ($M_{Ni} \approx 58.7$ u).

Compare these values with the energy uncertainty due to the lifetime according to (7.29) ($\tau_{Hg} \simeq 10^{-8}$ s, $\tau_{Ni} \simeq 10^{-14}$ s).

5.10 What is the temperature of a black sphere with a diameter of 10 cm which is emitting a total of 100 W thermal radiation? How much mass is lost each year by being radiated away?

Hint: Use the numerical values from (5.3).

5.11 Calculate the temperature of the sun and the energy density of the radiation in its interior, assuming that the sun is a spherical black body with a radius R of 7×10^8 m. The intensity of the solar radiation at the surface of the earth (which is 1.5×10^{11} m from the sun) is 1.4×10^3 W/m^2. Assume that the energy density in the interior of the sun is homogeneous. Is this realistic?

5.12 What is the wavelength of the spectral maximum of the radiation from a black body at 300 K (room temperature)? Calculate the monochromatic energy density at this frequency.

5.13 A photon releases a photoelectron with an energy of 2 eV from a metal which has a work function of 2 eV. What is the smallest possible value for the energy of this photon?

5.14 The work function for the photoeffect in potassium is 2.25 eV. For the case when light with a wavelength of 3.6×10^{-7} m falls on the potassium, calculate a) the braking potential U_{max} of the photoelectrons and b) the kinetic energy and the velocity of the fastest of the emitted electrons.

5.15 A homogeneous monochromatic light beam, wavelength 4.0×10^{-7} m, falls perpendicularly on a material with a work function of 2.0 eV. The beam intensity is 3.0×10^{-9} W/m^2. Calculate a) the number of electrons emitted per m^2 and second, b) the energy absorbed per m^2 and second, and c) the kinetic energy of the photoelectrons.

5.16 A metal surface is irradiated with light of various wavelengths λ. The braking potentials V indicated in the table are measured for the photoelectrons.

λ [10^{-7} m]	V [V]	λ [10^{-7} m]	V [V]
3.66	1.48	4.92	0.62
4.05	1.15	5.46	0.36
4.36	0.93	5.79	0.24

Plot the braking potential along the ordinate versus the frequency of the light along the abscissa. Calculate from the curve a) the threshold frequency, b) the photoelectric work function of the metal, and c) the quotient h/e.

5.17 The yellow D lines of sodium appear when sodium vapour is irradiated with electrons which have been accelerated through a potential difference of 2.11 V. Calculate the value of h/e.

5.18 In a Compton effect experiment, the scattered light quantum is observed at an angle of 60° to the direction of the incident light. After the collision, the scattered electron moves in a circular path with a radius $R = 1.5$ cm in a magnetic field $|\boldsymbol{B}| = 0.02$ Vs/m^2 which is perpendicular to the plane of the electron path. What is the energy and the wavelength of the incident light quantum?

Hint: Use (6.7) with $|\boldsymbol{E}| = 0$ to calculate the electron's path.

5.19 A photon with 10^4 eV energy collides with a free electron at rest and is scattered through an angle of 60°. Calculate a) the change in energy, frequency and wavelength of the photon, and b) the kinetic energy, momentum and direction of the electron after the collision.

5.20 X-rays with a wavelength of 1 Å are scattered on graphite. The scattered radiation is observed perpendicular to the direction of the incident x-rays.

a) How large is the Compton shift $\Delta\lambda$?
b) How large is the kinetic energy of the ejected electron?
c) What fraction of its original energy does the photon lose?
d) How large is the corresponding fraction of energy lost by a photon with a wavelength $\lambda = 0.1$ Å if it is deflected through 90° by Compton scattering?

The electron should be considered at rest before the collision, and the binding energy should be neglected.

5.21 A pulsed laser with a repetition rate of 20 Hz produces light pulses with a length of 30 ps (picoseconds). Its laser medium is Nd: YAG and the wavelength is 1064 nm. The light pulses are passed through a frequency-tripler (efficiency 10%, i.e. only 1/10 of the incident energy is available at the output of the frequency-tripler). An output pulse energy of 1 mJ is required at the output wavelength λ (to be calculated).

a) How many photons n are contained in an output pulse?
b) How high is the peak power P of the laser system at the output of the tripler?
c) What is the average light power I of the pulsed laser before the tripler, if only 0.1% of the electrical power is converted into light power?

6. The Electron

6.1 Production of Free Electrons

The name "electron", which is derived from the Greek word for amber, was coined by the English physicist *Stoney* in 1894.

In the early days of atomic physics, free electrons were usually produced as cathode rays from gas dicharges. Now, however, they are most often obtained using thermionic emission from wires. This process has the advantage that the electrons can easily be focussed and accelerated. Free electrons can also be produced by utilising the photo-effect (Chap. 5) or in the form of emissions from radioactive nuclei.

6.2 Size of the Electron

The electron is just as invisible as the atom; indeed, as a component of the latter, it must be smaller. We first arbitrarily define a parameter, called the classical electron radius, by making the following assumptions:

- the electron is a sphere with radius r_{el} and surface charge $-e$,
- the energy of the rest mass $E = m_0 c^2$ is equal to the potential electrostatic energy of the surface charge.

We use the formulae of classical electrostatics to calculate the electrostatic energy. The capacitance of a spherical surface of radius r is

$$C = 4\pi\varepsilon_0 r\,. \tag{6.1}$$

The work required to add a charge q to a capacitor with capacitance C is

$$W = \tfrac{1}{2} q^2/C\,. \tag{6.2}$$

Therefore the potential energy of a spherical capacitor, i.e. the energy of its electrostatic field, is

$$E_{pot} = \frac{e^2}{8\pi\varepsilon_0 r}\,. \tag{6.3}$$

The condition that $E_{pot} = m_0 c^2$ (m_0 is the rest mass of the electron and c is the velocity of light) determines the radius $r = r_{el}$:

$$r_{el} = \frac{e^2}{2 \cdot 4\pi\varepsilon_0 m_0 c^2}\,. \tag{6.4}$$

Other assumptions regarding the distribution of charge (e.g., continuous distribution of charge throughout the volume instead of a surface charge) lead to somewhat different numerical values. The "classical" electron radius is, finally, defined as

$$r_{el} = \frac{e^2}{4\pi\varepsilon_0 m_0 c^2} = 2.8 \cdot 10^{-15}\,\text{m}\,. \tag{6.5}$$

It can be seen from this derivation that the parameter is purely conceptual. Is it possible to measure the electron's radius? In principle, yes. For example, the scattering cross section can be determined by irradiating with x-rays, exactly as the scattering cross sections of gas atoms may be determined (Chap. 4). The result of such experiments is a cross section $\sigma = \pi \cdot r_{el}^2$, and the parameter r_{el} is found to be of the same order of magnitude as the classical electron radius defined above.

Experiments in which electrons are scattered by electrons reveal no deviations from the Coulomb law, even at very small collision distances. All results up to now have thus yielded only the information that the electron is a structureless, point-like particle.

6.3 The Charge of the Electron

As mentioned earlier, the charge of the electron, $-e$, can be derived from the Faraday constant F:

$$e = F/N_A\,. \tag{6.6}$$

However, since we wish to use this equation to determine Avagadro's number N_A, we require an independent method of measuring the elementary charge e.

This was accomplished by *Millikan*'s experiment (1911), in which the charge on small drops of oil is determined from their motion in the electric field of a capacitor. It remains the best method for determining e.

The principle of the method is illustrated in Fig. 6.1. Figure 6.2 shows the entire experimental setup. The rising or falling velocity of a charged oil droplet in the homogeneous electric field of a capacitor is determined by the resultant of all the forces acting on the droplet: electrostatic force, gravitational force, buoyancy in the air, and friction with the air. We will pass over the details of the measurement procedure; we mention only, as a curiosity, the fact that an incorrect value of the quantity e was used for some years due to an error in the determination of the viscosity of the air. The latter quantity is needed to calculate the frictional force acting on the droplet which is rising or falling. The best value of the elementary charge is currently $e = (1.6021917 \pm 0.0000070) \cdot 10^{-19}$ C.

The question has been repeatedly raised, whether there are smaller amounts of charge than the so-called elementary charge e. Up to the present time, no smaller charges have been detected unambiguously.

To explain the structure of elementary particles, the existence of more fundamental elementary particles, the "quarks", has been suggested; they would have charges of $e/3$ or $2e/3$. A number of experiments in high energy physics can, in fact, be understood by the assumption that such particles exist, but are bound to each other and/or to their anti-

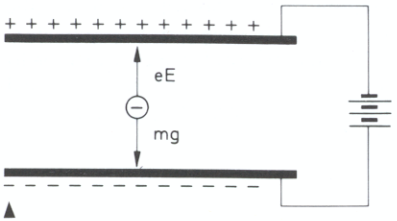

Fig. 6.1. Principle of the Millikan oil-drop experiment for measuring the charge of the electron. A negatively charged oil droplet experiences the force neE, where n is the number of elementary charges on the droplet; the graviational force mg acts in the opposite direction

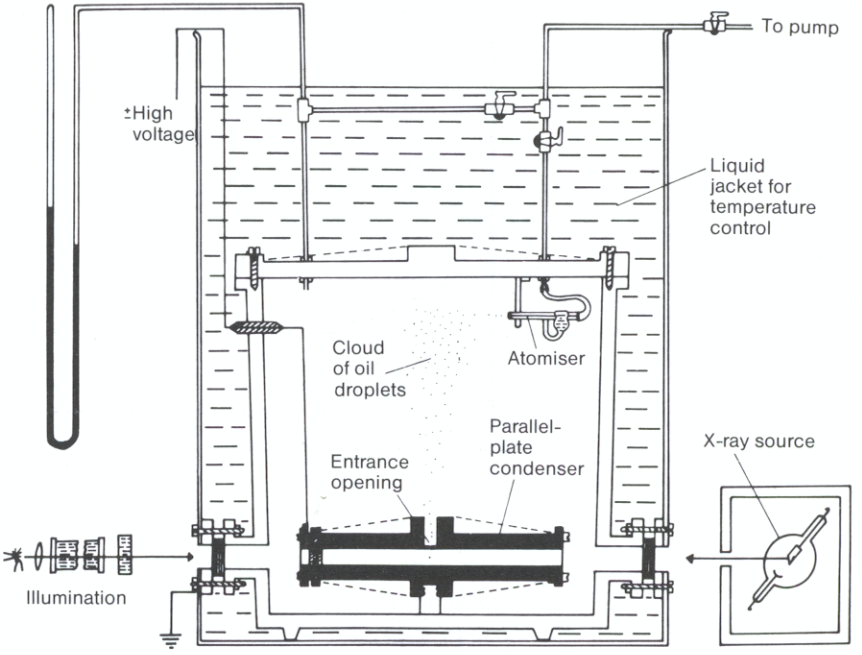

Fig. 6.2. Experimental arrangement of *Millikan* from Phys. Rev. **2**, 109 (1913). The oil droplets, which are formed by the atomiser, can be charged or discharged by irradiation with x-rays

particles. On the other hand, there has so far been no convincing proof of the existence of free quarks, and theoreticians have even developed a theory of "confinement". According to this theory, the forces between quarks become so large that they can never appear as individual particles.

6.4 The Specific Charge e/m of the Electron

The mass of the electron is determined by measuring the deflection of electrons in electric and magnetic fields. The motion is determined by the ratio of charge to mass e/m according to the equation

$$\boldsymbol{F} = m\frac{d\boldsymbol{v}}{dt} = -e[\boldsymbol{E} + (\boldsymbol{v} \times \boldsymbol{B})] \,. \tag{6.7}$$

Following the first e/m measurement by *Thompson* (1897), many methods for measuring this quantity were developed in the next 50 years, but all of them were basically variations of the same principle which we have already discussed for the parabolic method in mass spectroscopy.

The method of *Classen* (1907) is particularly elegant (Fig. 6.3). The $\boldsymbol{E}$ field between the cathode and the film imparts a uniform, known velocity to the electrons. The kinetic energy, to a non-relativistic approximation, is

$$\frac{m}{2} v^2 = eV \,, \tag{6.8}$$

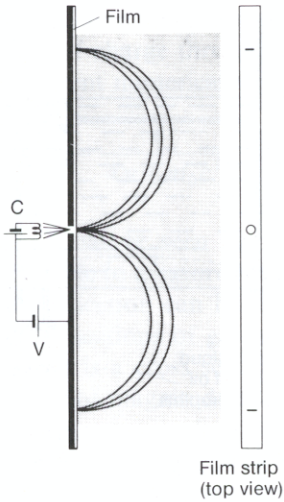

Fig. 6.3. Experimental arrangement for measurement of the specific mass m/e of the electron. The electrons are generated at the cathode C and accelerated by the voltage V. They are deflected into circular paths by a magnetic field perpendicular to the plane of the figure and recorded on a film. The direction of the deflection is reversed by reversing the poles of the magnet

where V is the accelerating voltage. Rearranging,

$$v = \sqrt{\frac{2eV}{m}} . \tag{6.9}$$

The $\boldsymbol{B}$ field deflects the electrons into a circular path with radius r. Equating the Lorentz and the centrifugal forces yields

$$\frac{mv^2}{r} = evB . \tag{6.10}$$

The desired ratio of charge to mass follows from (6.9) and (6.10):

$$\frac{e}{m} = \frac{2V}{r^2B^2} . \tag{6.11}$$

One can thus obtain the ratio e/m by measurement of a voltage, a magnetic field strength and a distance. Over the years, various other methods were used to measure the specific mass m/e. They differ primarily in the relative positions of the electric and magnetic fields. Figure 6.4 shows one of these other experimental arrangements, one which corresponds in principle to the Aston mass spectrograph.

The dependence of the mass on the velocity was examined quite early with the help of these experiments. Table 6.1 lists some measured values for e/m.

The limiting value of m as the kinetic energy of the electron went to zero was found to be $m_0 = 1.7588 \cdot 10^{-31}$ kg or $(5.485930 \pm 0.000034) \cdot 10^{-4}$ u. 1 u is thus 1822.84 m_0.

The dependence of the ratio e/m on the particle velocity was found experimentally in 1901 (4 years before *Einstein*'s theory of relativity) by *Kaufmann*. *Kaufmann* used the method known in mass spectroscopy as the Thomson parabola method (Figs. 3.2, 3). The particles are deflected in transverse $\boldsymbol{E}$ and $\boldsymbol{B}$ fields. The electrons studied by *Kaufmann* were β particles from radioactive sources, because his experiments were

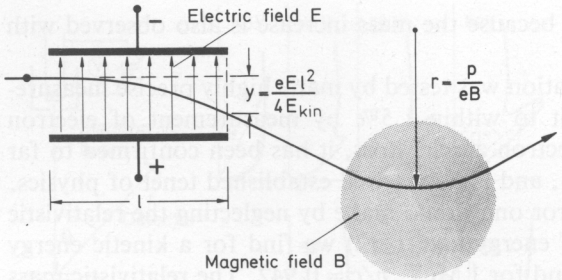

Fig. 6.4. Arrangement for measurement of the ratio e/m for electrons. Here the electrons are deflected first by an electric field and then by a magnetic field

Table 6.1. Specific charge of the electron at different accelerating voltage

Accelerating voltage V [kV]	0	500	1000	1500
Measured specific charge e/m [10^{11} C/kg]	1.76	0.88	0.56	0.44

meant to clarify the physical nature of β rays. However, the photographic record of the particles did not yield the segment of a parabola which would be expected if the ratio of e/m were constant at different velocities of the particles.

Kaufmann's curves can be understood in the following way: For a uniform value of e/m, each point of the parabola correspondings to a particular value of the velocity v. From the fact that a parabolic segment is actually observed for lower velocities (larger deflections), it can be concluded that the slower particles have a continuous velocity distribution at a constant mass. However, at high velocities v the mass appears to increase steadily. The curve therefore passes through points on each of a series of adjacent parabolas, corresponding to successively higher masses m.

These measurements were the first to substantiate the dependence of mass on velocity. They fit the Lorentz equation

$$m = m_0 \frac{1}{\sqrt{1 - v^2/c^2}} . \tag{6.12}$$

It was later shown that this equation can also be derived from the theory of relativity, if the validity and Lorentz invariance of the conservation of energy is assumed. The equation is equivalent to the principle $E = mc^2$. Figure 6.5 shows experimental values of the dependence of the mass on the velocity.

The following qualitative argument was advanced in an attempt to understand the change in mass with velocity: When the electron is accelerated, part of the energy is absorbed in the creation of the magnetic field of the moving electron – which is of course an electric current. Thus an "electromagnetic mass" is added to the inertial

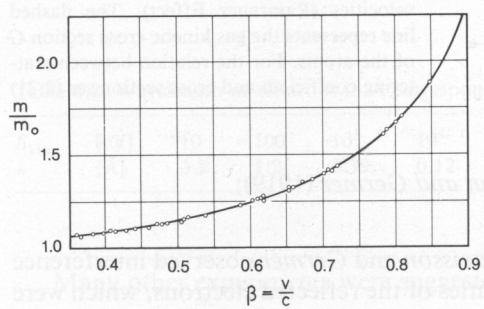

Fig. 6.5. Experimental values for the mass of the electron as a function of its velocity (test of the Lorentz formula). The mass m, in units of the rest mass m_0, is plotted against the velocity in units of the velocity of light, v/c

mass. This argument fails, however, because the mass increase is also observed with neutral particles, e.g. neutrons.

As time went on, the Lorentz equation was tested by many highly precise measurements. It was possible to confirm it to within 1.5% by measurement of electron energies under 1 MeV. In modern electron accelerators, it has been confirmed to far better precision, as shown in Fig. 6.5, and is now a well established tenet of physics.

It is instructive to consider the error one would make by neglecting the relativistic mass increase. From conservation of energy and (6.12) we find for a kinetic energy $E_{kin} = 1$ keV a velocity $v/c = 0.063$, and for 1 MeV, $v/c = 0.942$. The relativistic mass increase is then according to (6.12) at 1 keV $4 \cdot 10^{-3}$ times the rest mass m_0, but at 1 MeV it is already 2 times m_0, i.e. $(m - m_0)/m_0 = 2$.

6.5 Wave Character of Electrons and Other Particles

The motion of electrons in electric and magnetic fields may initially be understood as a particle motion. We have treated it as such in explaining various experiments up to now. There are, however, a number of different experiments in which electrons and other particles show interference and diffraction phenomena, that is they exhibit wave character. In this section, we will discuss the experimental grounds for assuming the existence of *matter waves*.

Experiment 1: The Ramsauer Effect (1921)

The measurement of the interaction cross section for collisions of extremely slow electrons with gas atoms yielded very small values, much smaller than those found in the kinetic theory of gases; at somewhat higher electron energies, the values were found to be much larger (Fig. 6.6). This type of minimum in the velocity dependence of the interaction cross section could be explained as the result of diffraction by particles whose size was comparable with the wavelength of the electrons.

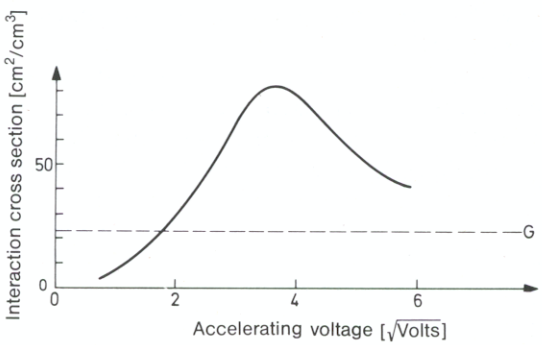

Fig. 6.6. Scattering coefficient $\alpha = n\sigma$ for electrons on gas atoms at various electron velocities (Ramsauer Effect). The dashed line represents the gas kinetic cross section G of the atoms. For the relation between scattering coefficient and cross section see (2.21)

Experiment 2: The Investigations of Davisson and Germer (1919); *Their Explanation* (1927)

On reflecting slow electrons from crystals, *Davisson* and *Germer* observed interference effects, i.e. maxima and minima in the intensities of the reflected electrons, which were

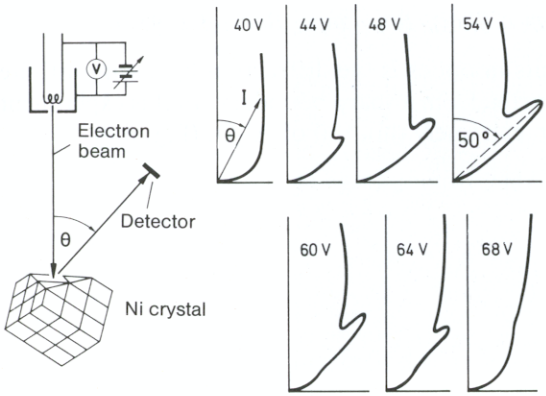

Fig. 6.7. Electron interference experiment of *Davisson* and *Germer*. *Left:* Diagram of the apparatus. The electrons accelerated through the voltage V are reflected from selected surfaces of a single crystal of nickel and recorded as a function of the reflection angle θ. *Right:* Angular distribution of reflected electrons at various accelerating voltages. The diagrams shown are polar plots in which the distance from the zero point to the curve corresponds to the intensity of reflection at the corresponding angle. There is a maximum at a scattering or reflection angle of about 50°, due to interference

uniquely determined by the electron velocities, the crystal orientation, and the angle of observation. Their experimental setup and the results are shown schematically in Fig. 6.7. The interference maxima and minima come about in a manner similar to x-ray diffraction from the lattice planes of a crystal (Bragg reflections, see Sect. 2.4.5). The occurrence of interference means that the motion of the electrons must be connected with a wave phenomenon. Indeed, *de Broglie* put forth the suggestion that just as light can possess a particle character, electrons must also have a wave character; he assumed the validity of the fundamental relation $p = h/\lambda$ between the momentum and the wavelength.

If we express the momentum by means of the mass and the velocity, i.e. $p = m_0 v$, and set $v = \sqrt{2E_{\text{kin}}/m_0}$ for non-relativistic velocities, we find

$$\lambda = h/\sqrt{2m_0 E_{\text{kin}}} \,. \tag{6.13}$$

It follows that for electrons which have been accelerated by a voltage V,

$$\lambda = \frac{12.3}{\sqrt{V}} \,[\text{Å}] \,.$$

The wavelength is measured in angstroms and the kinetic energy is converted to eV, because the electrons acquire their kinetic energy by traversing a voltage V. An accelerating voltage of 54 V, for example, produces $\lambda = 1.67$ Å.

De Broglie's hypothesis applies to all particles, not only electrons. The values given in Table 6.2 are for electrons.

Table 6.2. Wavelength of electrons in Å corresponding to various energies [eV], according to *de Broglie*

E_{kin}	[eV]	10	100	10^3	10^4	10^5	10^6	10^7	10^8
λ	[Å]	3.9	1.2	0.39	0.12	$3.7 \cdot 10^{-3}$	$8.7 \cdot 10^{-3}$	$1.2 \cdot 10^{-3}$	$1.2 \cdot 10^{-4}$

Many other experiments were suggested and could now be understood.

Experiment 3: Fresnel Diffraction from a Sharp Boundary, Boersch (1956)

One of the basic diffraction experiments in optics is the diffraction by a semi-infinite plane. Like light, electrons can be diffracted from a sharp boundary. In this experiment they are diffracted from the edge of an extremely thin foil of Al_2O_3 (Fig. 6.8).

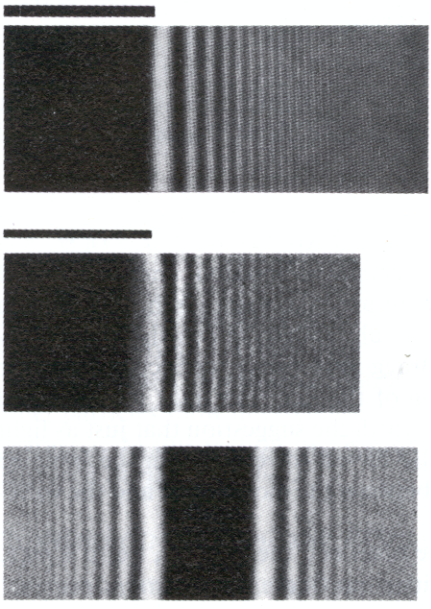

Fig. 6.8. *Above:* Diffraction lines of filtered red light at the geometric shadow boundary of a semi-infinite plane. *Middle:* Diffraction of electrons from the edge of an Al_2O_3 foil in a semi-infinite plane. $\lambda = 5 \cdot 10^{-12}$ m, corresponding to an electron energy of $3.4 \cdot 10^4$ eV. *Below:* Diffraction of electrons from a 2 μm thick gold-coated wire. Electron energy $1.94 \cdot 10^4$ eV. All photos from R. W. Pohl, *Optik und Atomphysik*, 11, 12th ed. (Springer, Berlin, Heidelberg, New York 1967) Figs. 202, 522, 523

Experiment 4: Diffraction from a Fresnel Double Prism, Möllenstedt (1956)

The Fresnel double prism experiment of classical optics was carried out with electrons. In this experiment, an electrically charged quartz fibre acts a double prism for electrons. Electrons from the two virtual electron sources interfere (Fig. 6.9). Measurement of the resulting interference lines in the image plane confirmed the de Broglie relationship to within 0.5% (Fig. 6.10).

Experiment 5: Atoms as Waves (1931)

The wave character of particles other than electrons was also demonstrated by interference experiments. *Stern*, *Frisch* and *Estermann* (1931) observed the diffraction of beams of helium atoms from the surface of a LiF crystal. The wavelength of the helium atoms is derived from the temperature $T = 400\,\mathrm{K}$ and the mean kinetic energy $\bar{\varepsilon} = 3\,kT/2$ of the atomic beam. It lies in the angstrom range:

$$\lambda_{\mathrm{He}} = h/\sqrt{2mE} = h/\sqrt{3\,m_{\mathrm{He}}kT}\,.$$

This relationship has also been experimentally confirmed.

Interference and diffraction with particle beams are now included among the routine physical methods. Electrons can be used in the same interference experiments as x-rays.

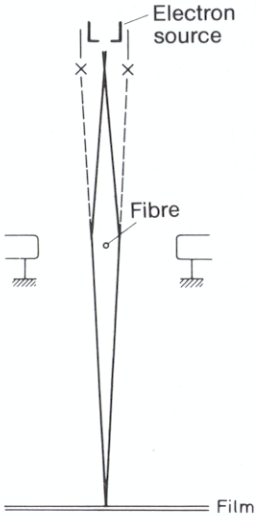

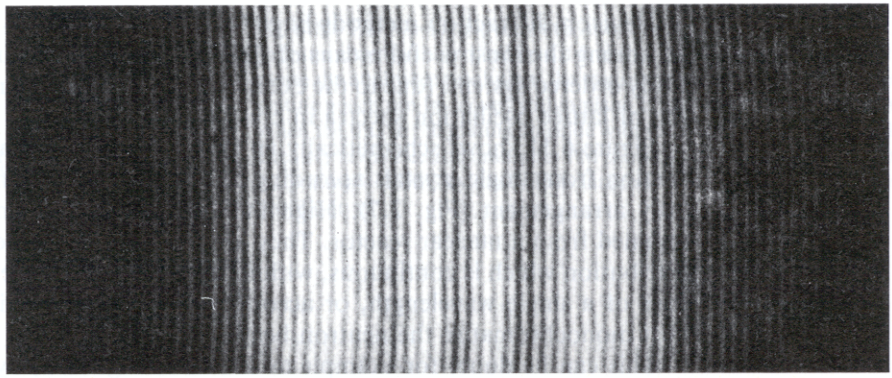

Fig. 6.10. Electron interference from the electrostatic double prism according to *Möllenstedt* and *Düker*. This image shows the measured intensity distribution on the film in Fig. 6.9; from Gerthsen, Kneser, Vogel: *Physik*, 13th ed. (Springer, Berlin, Heidelberg, New York 1977)

Fig. 6.9. Electron interference with an electrostatic double prism according to *Möllenstedt* and *Düker*. There is a voltage between the fibre and the counterelectrodes. The electrons are deflected by the resulting inhomogeneous field as shown. From Gerthsen, Kneser, Vogel: *Physik*, 13th ed. (Springer, Berlin, Heidelberg, New York 1977) Fig. 10.68

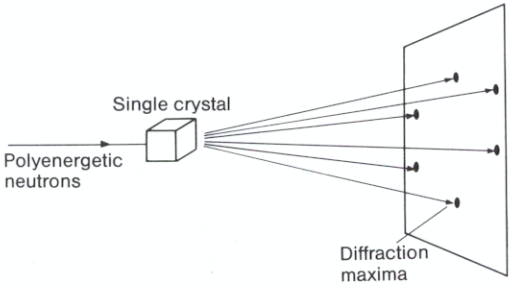

Fig. 6.11. Neutron diffraction from a single crystal, von Laue arrangement. With polyenergetic neutrons, one obtains Laue diagrams from scattering on the single crystal

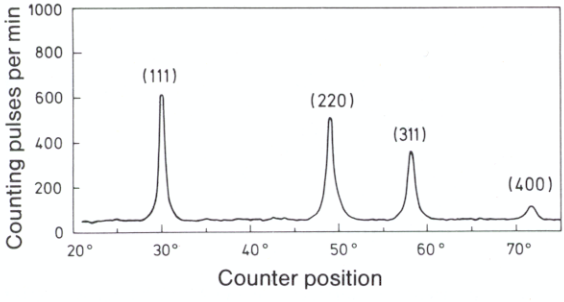

Fig. 6.13. Neutron diffraction from diamond powder, according to *G. Bacon*. Diffraction maxima occur from four families of lattice planes, which are denoted by the crystallographic indices (111), (220), (311) and (400)

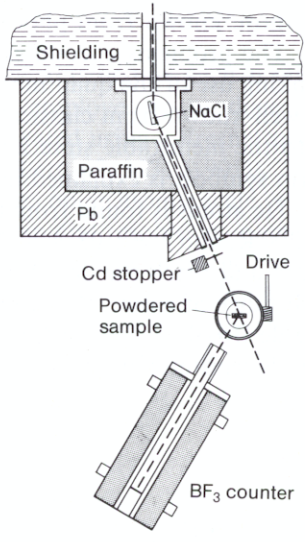

Fig. 6.12. Neutron spectrometer according to E. V. Wollan, C. G. Shull, Phys. Rev. **73**, 830 (1948). The neutrons are monochromatised by reflection from a NaCl crystal. When diffracted from a polycrystalline sample, they generate interference rings according to *Debye-Scherrer*. They are measured by means of a BF_3 counter

Neutron diffraction methods have become important in solid state physics. They are among the most useful means of determining crystal structures, analysing magnetically ordered systems (due to the existence of a neutron magnetic moment), and detection of lattice oscillation spectra in crystals.

Figure 6.11 shows schematically an arrangement for measurement of neutron diffraction from single crystals according to *von Laue*. It is completely analogous to the x-ray arrangement (Fig. 2.7). High intensity neutron beams are most conveniently obtained from a nuclear reactor. They are produced by nuclear fission with a velocity distribution which is continuous, within certain limits. If one wishes to work with particles of a single wavelength, or according to *de Broglie*, with uniform velocity, one must monochromatise the neutron beam.

This can be done, for example as shown in Fig. 6.12, by reflection from a single crystal (here NaCl). If these monochromatic neutrons are directed onto a polycrystalline or powdered sample, one obtains the same interference patterns as with the Debye-Scherrer x-ray technique (Fig. 2.10). An example of such a pattern is shown in Fig. 6.13; it is the result of diffraction of a neutron beam from diamond powder.

6.6 Interferometry with Atoms

The wave nature of particles can be employed to construct an interferometer using atomic beams, or to set up an imaging system based on interference of atoms, similar to those known from photon optics.

The problems encountered in this *atomic interferometry* can be demonstrated by making use of the quantum-mechanical analog of *Young's* two-slit experiment, which is well-known from classical optics; see Fig. 6.14. A beam of helium atoms is excited into the metastable state 2^1S_0 or 2^3S_0 by electron bombardment (the meaning of the term symbols is explained in Sect. 17.1). The corresponding de Broglie wavelength of the He atoms is found from (6.13) using the velocity of the He atoms to be $\lambda = 0.56$ Å at 300 K, and $\lambda = 1.03$ Å at 77 K. The excited atoms now pass through a slit A of width 2 μm and reach the double slit B. It consists of two slits of width 1 μm separated by a distance of 8 μm. The atoms which pass through these two slits, i.e. the corresponding de Broglie waves, interfere in the region behind *B*. The resulting interference pattern is registered in the plane *C* by a photoelectron multiplier, which measures the light

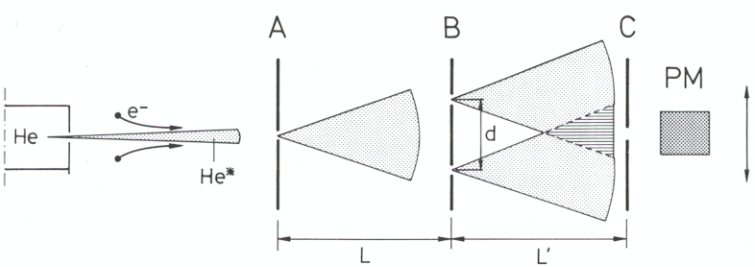

Fig. 6.14. The experimental setup for carrying out *Young's* two-slit interference experiment with atoms (after O. Carnal and J. Mlynek, Phys. Rev. Lett. **66**, 2689 (1991)). A beam of helium atoms is excited by electron bombardment and passes through a slit 2 μm wide in plane A, then reaches plane B containing two slits of width 1 μm and spacing 8 μm. The resulting interference pattern behind plane B is observed via a third slit in plane C using a secondary electron multiplier (PM)

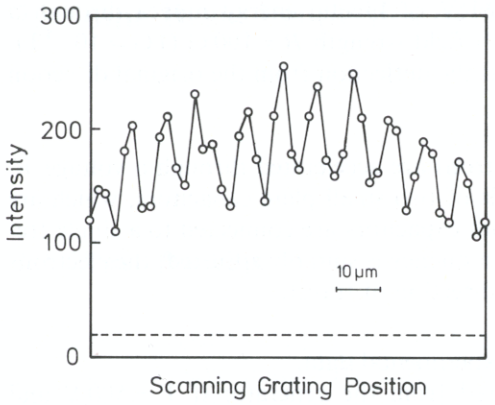

Fig. 6.15. The two-slit experiment in atomic interferometry carried out with the experimental setup shown in Fig. 6.14: the intensity distribution in plane C. To increase the attainable resolution, the measurement is performed using a mechanical grating which can be moved within plane C and has the "correct" lattice spacing. When the slits in the grating coincide with the interference maxima, the measured intensity at the electron multiplier PM shows a maximum; it is at a minimum when the grating is shifted by one-half its lattice-spacing period. The lattice spacing here was 8 μm

emitted by the metastable He atoms as they return to their ground states. Figure 6.15 shows the result of such a measurement. One observes a system of equidistant interference maxima separated by a distance which corresponds to what one would calculate from the geometry of the experiment and the de Broglie wavelength of the atomic beam. This provides an impressive proof of the wave nature of atoms and the validity of (6.13).

The biprisma experiment, in which an electrically-charged wire serves as interferometer (cf. Fig. 6.9), has also been carried out with atoms and was used to determine their de Broglie wavelengths [S. Nowak, N. Stuhler, T. Pfau, and J. Mlynek: Phys. Rev. Lett. **81**, 5792 (1998)].

In this manner, the diffraction of atoms by micromechanical structures such as mirrors, lenses, and beam splitters for matter waves can be employed to produce an 'atomic optics'. Image formation has already been demonstrated using a Fresnel zone plate, for example (O. Carnal, J. Mlynek et al., Phys. Rev. Lett. **67**, 3231 (1991)). The way has thus been opened for the construction of microprobes on an atomic scale, with which one could, for example, study surfaces with a high spatial resolution, namely that of the de Broglie wavelength, and nondestructively. Since the energy of the atoms can be made very small, less than 10 meV, little radiation damage would be produced on the surface under investigation. The high spatial resolution is made possible by the short wavelengths. This area of atom lithography is certainly an interesting field for future research.

Problems

6.1 In the Millikan experiment to determine the elementary charge, a voltage of $V = 50$ V is applied between the plates of a capacitor, which are 1 cm apart. What must the diameter $2r$ of the oil droplets be, in order that a droplet with a single charge is held in suspension? What is the velocity v of the droplets as they fall when the direction of the electric field is reversed? The coefficient of viscosity of air is $\eta = 1.84 \times 10^{-4}$ poise, and the density of the oil $\varrho = 0.9\ \mathrm{g/cm^3}$.

Hint: The frictional force F_R is given by Stokes' Law, $F_R = -6\pi\eta r v$ (1 poise = 1 dyn s/cm^2 = 10^{-1} Ns/m^2).

6.2 A singly charged particle with 0.12 MeV of kinetic energy moves through a transverse homogeneous magnetic field with field strength $B = 100$ G ($1\,\text{G} = 10^{-4}\,\text{T}$). Calculate the mass of the particle, given that the deflection from the original direction of travel is 3 mm in a 10 cm flight path.

6.3 To measure their specific charge, electrons are accelerated through a voltage V. Then they pass through the transverse fields of two small plate capacitors, which are placed at a distance l from one another. Both capacitors are connected to a single frequency generator (frequency ν). When the frequency is suitably adjusted, the electrons leave the second capacitor in their original direction of travel.

a) Under what condition is this possible?
Derive a relation between e/m and the experimental data.
b) What is the minimum frequency required from the generator if $V = 500$ V and $l = 10$ cm?
c) Sketch the apparatus.

6.4 If the kinetic energy of an electron is equivalent to its rest mass, what is its velocity?

6.5 The rest energy of the electron is 0.511 MeV. Give the ratio of inertial mass to rest mass for an electron as a function of its kinetic energy. How large is the ratio for $E_{\text{kin}} = 1$ MeV?

6.6 Calculate the de Broglie wavelength of an electron with the velocity $v = 0.8\,c$, using relativistic relationships.

6.7 Calculate the de Broglie wavelength of an electron with kinetic energy of 1 eV, 100 eV, 1000 eV, 100 keV. Which wavelengths will be noticeably diffracted in a nickel crystal, in which the atomic spacing is about 2.15 Å? Calculate the kinetic energy of those electrons which are scattered through angles of less than 30°.

6.8 What is the average kinetic energy and the corresponding de Broglie wavelength of thermal neutrons, i.e., neutrons which are in thermal equilibrium with matter at 25 °C? According to the Bragg formula, what is the angle of incidence at which the first interference maximum occurs when these neutrons are reflected from a NaCl crystal in which the lattice spacing d is 2.82 Å? The mass of the neutron is 1.675×10^{-27} kg.

6.9 Consider an electron which is far away from a proton and at rest. It is attracted to the proton. Calculate the magnitude of the wavelength of the electron when it has approached within a) 1 m and b) 0.5×10^{-10} m of the proton. (The latter distance is of the same order as the orbital radius of the electron in the ground state of the hydrogen atom.)